



PCCP

**Full-Dimensional Schrödinger Wavefunction Calculations
using Tensors and Quantum Computers: the Cartesian
component-separated approach**

Journal:	<i>Physical Chemistry Chemical Physics</i>
Manuscript ID	CP-ART-05-2021-002036.R2
Article Type:	Paper
Date Submitted by the Author:	15-Jan-2022
Complete List of Authors:	Poirier, Bill; Texas Tech University, Chemistry and Biochemistry Jerke, Jonathan; Texas Tech University, Chemistry and Biochemistry

SCHOLARONE™
Manuscripts

Cite this: DOI: 00.0000/xxxxxxxxxx

Full-Dimensional Schrödinger Wavefunction Calculations using Tensors and Quantum Computers: the Cartesian component-separated approach

Bill Poirier^{*a} and Jonathan Jerke^b

Received Date

Accepted Date

DOI: 00.0000/xxxxxxxxxx

Traditional methods in quantum chemistry rely on Hartree-Fock-based Slater-determinant (SD) representations, whose underlying zeroth-order picture assumes separability by *particle*. Here, we explore a radically different approach, based on separability by *Cartesian component*, rather than by particle [*J. Chem. Phys.*, 2018, **148**, 104101]. The approach appears to be very well suited for 3D grid-based methods in quantum chemistry, and thereby also for so-called “first-quantized” quantum computing. We first present an overview of the approach as implemented on classical computers, including numerical results that justify performance claims. In particular, we perform numerical calculations with four explicit electrons that are equivalent to full-CI matrix diagonalization with nearly 10^{15} SDs. We then present an implementation for quantum computers for which the number of quantum gates (and to a lesser extent, the number of qubits) can be dramatically reduced, in comparison with other quantum circuitry that has been envisioned for implementing first-quantized “quantum computational chemistry” (QCC).

1 Introduction

The importance of quantum chemistry simulations^{1–4} across a broad swathe of science and engineering lies beyond question. In the field of *quantum computational chemistry* (QCC)—i.e., quantum chemistry run on quantum computers^{5–35}—most efforts to date have attempted to simply “translate” as much as possible of the standard electronic structure methodology, developed over many decades for classical computers. Given the vast and fundamental differences between quantum and classical architectures, however, this may not be the most profitable or natural approach.

In particular, standard methods (what in QCC parlance are called “second-quantized,” in a sense to be defined shortly) rely on Hartree-Fock (HF) (or other) Slater-determinant (SD) basis set representations.^{1–3,7,8,27,35} The underlying zeroth-order picture assumes separable products of single-particle molecular (spin)-orbital functions. Depending on the further approximations used by the particular implementation, standard methods are typically:

- (a) not always reliably accurate for strongly correlated systems (except in a full-CI matrix calculation that can be difficult to achieve in practice).
- (b) generally not designed to compute many accurate excited

electronic states (i.e., tens or hundreds of states, including position-dependent wavefunctions).

- (c) usually (but not always³⁶) applied only to the pure electronic structure for a given molecular geometry, not to the combined electron-nuclear motion quantum many-body problem describing the total molecule.
- (d) not universally regarded as the most competitive candidates for long-term, full-fledged quantum computation.

By “full-fledged quantum computation,” we mean calculations that are performed entirely on a *bona fide* quantum computer, without assistance from a classical computer. “Long term” refers to fault-tolerant error-corrected quantum computing, on a scale that lies beyond the reach of present-day NISQ (noisy intermediate-scale quantum) computing hardware.^{37,38}

In the QCC context, standard second-order methods are currently being pursued as an important near-term strategy—e.g., for use on hybrid quantum/classical computing platforms.^{24,25,28,29,35} By its nature, hybrid computing is limited in terms of “quantum supremacy”^{13,18,31,35}—by which is meant computing well beyond the capabilities of the most advanced classical computers. For the long term, it has been argued by some well-known leaders in the field that the most effective QCC algorithms are likely to be *first-quantized* strategies^{8–15,20–23,26,31,35}—i.e., those that rely on explicit coordinate-grid-based representations of the entire electronic (or electron-

^a Department of Chemistry and Biochemistry and Department of Physics, Texas Tech University, P.O. Box 41061, Lubbock, Texas 79409-1061, USA. Fax: 806-742-1289; Tel: 806-834-3099; E-mail: Bill.Poirier@ttu.edu

^b Email: jonathanjerke@aya.yale.edu

nuclear) wavefunction, across all system coordinates. Some reasons for this assessment are presented below, although the interested reader is directed to the references above for further explanation. In any event, the “jury is still out” until such time as fault-tolerant quantum computers have come on the scene—by which point there will undoubtedly be further algorithmic developments that will have taken place as well.

Note that we are using “first-” and “second-quantized” in the QCC sense,^{7,8,27,35} which differs slightly from standard electronic structure usage,^{1–3} as has caused some confusion in the past. To make matters worse, in the QCC context, the term “first-quantized” can also be used to describe plane-wave and more sophisticated basis set representations, similar to the molecular orbitals of the second-quantized approach. However, *insofar as QCC and this paper are concerned*, the defining feature of any “second-quantized” calculation is its reliance on an SD basis representation. First-quantized methods are not constrained in this manner, and not subject to the limitations (a) through (d) above. Further clarifying discussion on first- vs. second-quantized calculations, and the CCS approach, may be found in the Appendix.

In comparison with second-quantized methods, the chief drawbacks of first-quantized methods are that: (i) *much* larger basis set sizes are typically needed to represent the electronic wavefunction (at least for grid-based representations), and; (ii) antisymmetry is not “built in” from the start, but must be explicitly imposed. These present very substantial obstacles on classical computers, so much so such that to date, only a few serious attempts have been made to develop viable first-quantized electronic structure methods (mostly in the context of two-electron basis functions or geminals).^{39–43} The primary reason is the implied exponential scaling of computational resources with respect to the number of particles (N), or system dimensionality ($3N$).

On true quantum computers, however—at least as they are currently envisioned to exist within a few years—neither drawback (i) nor (ii) above is expected to be especially daunting. With regard to (i), the exponential scaling becomes *linear* scaling, in terms of the “space complexity,” or total number of logical qubits required to store the wavefunction. More specifically, storing the wavefunction will require something like $3Nn$ logical qubits (ignoring ancilla qubits, error correction qubits, etc.), with a minimum of $n \approx 7$. Likewise, the “gate complexity” or algorithmic scaling is at worst $O(N^2)$. As for (ii), this is taken up in Sec. 2.3.

It has also been argued that first-quantized calculations are more accurate than second-quantized (apart from full-CI) calculations, as fewer approximations and assumptions are used.^{33–35} Even if largely true, this author is not fully convinced by such arguments; in particular, grid-based calculations can introduce errors of their own—e.g., via quadrature approximation^{44–50} (see also Sec. 4.2). On the other hand, it is certainly true that removing the SD constraint from the basis set opens the door to new types of highly efficient representations for handling strongly correlated systems, as deserves further exploration (Sec. 2.3).

First-quantized methods also enable direct treatment of the combined electron-nuclear motion quantum many-body problem³⁵ (although recently, second-quantized methods have also been modified to do so³⁶). This feature turns out to be *vital*ly im-

portant in the QCC context, owing to the fact that separate electronic and nuclear motion calculations require large-dimensional potential energy surfaces, whose explicit calculation itself scales exponentially—even on a quantum computer.^{14,17,35}

On the other hand, the tremendous promise of first-quantized QCC is mitigated by the limits of present-day NISQ hardware, which can accommodate no more than ~ 100 or so qubits in total³⁵—to say nothing of gate complexity and depth restrictions imposed by current gate fidelities.^{25,27,28,35,37,38,51} For realistic QCC applications, the circuit complexities required by first-quantized methods are still beyond what can be accommodated in the near-term future. Nevertheless by developing better first-quantized QCC algorithms today—i.e., with improved scaling, higher accuracy, fewer required qubits and quantum gates, etc.—we will arrive that much sooner at the desired tomorrow.

Recent efforts in first-quantized QCC development have concentrated on improving scaling and scalability,^{22,24–26,28,35} and on efficient strategies for implementing the requisite unitary evolutions [e.g., linear combination of unitary (LCU) operators].^{26,35,52–54} Additionally, Galerkin discretization offers a rigorously variational approach with respect to basis size,^{24,26,35} by eliminating all quadrature error. Such techniques represent the current state of the art, even when grid or plane-wave representations are used (second-quantized QCC has met with more success, to date, in terms of specialized orbitals/basis sets^{15,27,35,54–56}).

The present work approaches first-quantized QCC from a complementary direction—by exploiting alternate representations that require fewer qubits, and that also give rise to quantum circuits with *far* fewer quantum gates. Specifically, we employ a radically different, tensor-product representation of the exact Coulomb potential energy operators, based on separability by *Cartesian component* rather than by particle.^{50,57,58} The resultant “Cartesian component-separated” (CCS) approach is first-quantized (by the definition given above), and otherwise turns out to resolve all of the limitations (a)–(d) (as listed above).

On classical computers, the CCS tensor-product representation of the Hamiltonian may be combined with a similar tensor-product form for the wavefunction—giving rise to a highly efficient computational quantum chemistry scheme, exhibiting many orders-of-magnitude reduction in numerical effort, as compared to explicit representations. Using only grid or plane-wave basis sets, classical CCS calculations have been performed to compute multiple excited electronic states (including wavefunctions) for atoms up to lithium,^{57,59} for other central-force applications with non-Coulomb interactions,⁵⁸ and for strongly correlated electron gases with up to $N = 4$ explicit electrons.^{60–63} The method is also currently being applied to solve the combined electron-nuclear motion problem^{14,17,35} (for H_2^+ ⁶⁴ and H_2 ⁶⁵).

To further demonstrate the feasibility of the classical CCS approach, we perform here an explicit $N = 4$ calculation of the “harmonium” central-force system,^{58,66–68} using only a plane-wave representation. The underlying basis size required is astronomical—i.e., $N_B \approx 10^{15}$. This calculation may be compared with a full configuration interaction (full-CI) matrix diagonalization conducted using a similar number of SD basis functions, and with $M \approx 5000$ single-particle (spin-)orbitals. Such classical CCS

calculations are important not only in their own right, but also to establish accurate benchmarks for future first-quantized QCC calculations—particularly those using grid or plane-wave basis representations. For example, from such classical CCS calculations, we can estimate that something like $n \approx 7$ logical qubits will typically be required per degree of freedom (Sec. 4.1).

On the other hand, the classical CCS calculations conducted to date may all be regarded as “preliminary,” in the sense that they have all used a very poor choice of basis that does not exploit CCS’s primary advantages vis-à-vis correlation. In this paper, for the first time, we set the theoretical stage for “optimized” CCS representations (analogous to Hartree-Fock) that take maximum advantage of correlation, and may thus give rise to orders-of-magnitude reductions in the *underlying* basis size, N_B —irrespective of the subsequent tensor-product reductions that classical CCS also provides. Such developments are expected to greatly improve what classical CCS may ultimately be able to do—with respect to system size N , overall numerical accuracy, or both.

The remainder of this paper is as follows. In Sec. 2, we lay out the advantages and operation of the first-quantized CCS approach in more detail, discussing also the form of the tensor-product representations used for both the Hamiltonian operators and the wavefunctions. This section concludes with a discussion of permutation symmetry, and how to rigorously enforce the condition of antisymmetry. Sec. 3 analyzes various classical CCS results that have been obtained to date (including the brand new results for $N = 4$ harmonium), with an eye towards what these imply about the likely capabilities of the CCS approach in future, both in the classical and quantum computing contexts. Sec. 4 then lays out our proposed quantum circuitry for implementing CCS as a QCC method—encompassing both time-independent eigenstate solutions as well as time-dependent solutions.

Although it is highly likely that a CCS QCC approach could be applied in conjunction with more sophisticated unitary evolution strategies such as LCU,⁵⁶ for pedagogical simplicity, we address here only the more standard and straightforward “canonical Trotter method.”^{9,12,18,28,35,69} In this context, we can realize a significant reduction in space complexity, and a *vast* reduction in gate complexity, in comparison with other first-quantized quantum circuitry that has been envisioned for QCC. Two alternate CCS implementations are presented, providing a potentially useful “engineering tradeoff” between space and gate complexities.

2 Methodology

In this section, we present the most *generalized* version of the CCS theory—i.e., which does *not* presume separability by particle, and therefore allows for substantial correlation to be built directly into the representational basis itself. Although this is the most important and distinctive feature of the CCS approach, all classical CCS calculations performed to date^{50,57,58,63} have used sinc or plane wave basis sets, which are separable with respect to *both* particle *and* Cartesian component. Such basis sets have provided a natural starting-off point for classical computations, and will also form the basis of our (initial) QCC algorithm in Sec. 4. On the other hand, the past emphasis on plane-wave—or at least particle-separated—basis sets may have also served to obscure the

greater significance of CCS. That situation will be rectified here.

2.1 CCS Explicit and Tensor SOP Representations of the Wavefunction

For a system of N electrons, let $\vec{r}_i = (x_i, y_i, z_i)$ represent the Cartesian components of the i ’th electron position. We shall work with a general CCS representational basis of the form

$$\Phi_{\vec{m}}(\vec{r}_1, \dots, \vec{r}_N) = X_{m_x}(x_1, \dots, x_N) Y_{m_y}(y_1, \dots, y_N) Z_{m_z}(z_1, \dots, z_N), \quad (1)$$

where $\vec{m} = (m_x, m_y, m_z)$. Note that the basis spans the entire $3N$ -dimensional configuration space. The form of Eq. (1) should be contrasted with the standard SD form. Apart from antisymmetrization, SDs are separable by *particle*, whereas Eq. (1) is separable only by *Cartesian component*. This means that full correlation across (in principle) all N electrons can be built directly into the basis representation. On the other hand, Eq. (1) does not (yet) incorporate either permutation symmetry or spin.

The total size of the representational basis of Eq. (1) is $N_B = M_x M_y M_z$, where M_d is the basis size for the d ’th Cartesian component (i.e., $d = \{x, y, z\}$), so that $1 \leq m_d \leq M_d$. Alternatively, M_d may be thought of as the number of CCS “orbitals” associated with the d ’th Cartesian component—which need not be the same for x , y , and z . Obviously, M_d increases quickly with N , even if an excellent, highly efficient basis is chosen. For the (typically) worst-case choice of a plane wave (or sinc) basis, we have (e.g., for the x component),

$$X_{m_x}(x_1, \dots, x_N) = \phi_{m_{1x}}^x(x_1) \cdots \phi_{m_{Nx}}^x(x_N), \quad (2)$$

with $m_x = (m_{1x}, \dots, m_{Nx})$, etc. If $1 \leq m_{id} \leq L$, so that there are L basis functions per Cartesian component *per particle*, then the number of CCS orbitals per component is $M_d = L^N$, and the total basis size is $N_B = L^{3N}$.

For molecular applications treating core electrons exactly, $L \approx 100$ might be a typical value. In comparison with the second-quantized SD approach, this would correspond to $M = L^3 \approx 10^6$ single-particle orbitals—a “worst-case” choice of basis indeed! Recognizing further that explicit matrix representations would require storage of $N_B^2 = L^{6N}$ elements in all, it becomes clear that even two-electron applications lie beyond what would be possible on any classical computer. Use of smarter CCS basis sets, *not* of the Eq. (2) form, can of course greatly reduce the requisite M_d and N_B sizes, thereby effectively increasing the number of electrons that might be treated explicitly. In any case, it is clear that the scaling of explicit vector and matrix representations with respect to N poses a severe challenge for classical computers.

It is at this juncture, then, that the classical and quantum computational strategies part company—at least with respect to how the N -electron CCS wavefunction is actually represented numerically. On the quantum side, the exponential growth of N_B with N does not pose a fundamental problem; as discussed, this corresponds to *linear* growth in the number of qubits (Sec. 4). We therefore simply use the explicit vector representation of the N -

electron wavefunction implied by Eq. (1), i.e.,

$$\Psi(\vec{r}_1, \dots, \vec{r}_N) \approx \sum_{m_x=1}^{M_x} \sum_{m_y=1}^{M_y} \sum_{m_z=1}^{M_z} \Psi_{m_x m_y m_z} \Phi_{\vec{m}}(\vec{r}_1, \dots, \vec{r}_N), \quad (3)$$

[together with Eq. (2)], as is. More specifically, in the present QCC CCS implementation, both plane wave and sinc representations are used, with explicit storage of the vector, $\Psi_{m_x m_y m_z}$, requiring $N_B = L^{3N}$ elements, as discussed. [As per Sec. 4, the quantum Fourier transform^{11,12,70} (QFT) is used to switch between these two representations.]

In contrast, the classical CCS implementation replaces the explicit vector representation of Eq. (3) with the following [generic Eq. (1) basis] tensor “sum of product” (SOP) form:

$$\Psi_{\Lambda}(\vec{r}_1, \dots, \vec{r}_N) \approx \sum_{\lambda=1}^{\Lambda} \sum_{m_x=1}^{M_x} \sum_{m_y=1}^{M_y} \sum_{m_z=1}^{M_z} X_{m_x}^{\lambda} Y_{m_y}^{\lambda} Z_{m_z}^{\lambda} \Phi_{\vec{m}}(\vec{r}_1, \dots, \vec{r}_N) \quad (4)$$

In Eq. (4), the number of elements to be stored is now only $\Lambda(M_x + M_y + M_z)$ —which, in general, is only a tiny fraction of N_B . Of course—as with all tensor methods—this requires that a sufficiently good wavefunction approximation is achievable using a reasonably small number of terms, Λ . For all CCS applications to date, this has been achieved with Λ on the order of 100.^{50,57,58,63} Consequently, explicit N -electron wavefunctions have been stored using only a modest amount of RAM on classical computers—even up to $N = 4$.

Such enormous reductions are not atypical when tensor SOPs are employed. Recent years have seen an explosion in the use of modern tensor methods across a vast range of data science applications, as a tool for drastically reducing data storage requirements.^{71–73} Even in the electronic structure realm, use of tensor SOPs to represent the electronic state is not new, and has been applied to great effect for a number of years now.^{74–78} Nevertheless, our use of tensor SOPs is radically different from earlier efforts, in two important ways. To begin with, it is applied across a CCS basis that is in general separable only by Cartesian component [Eq. (1)] and not by particle. The very nature of the tensor products involved is thus quite different from previous efforts based on particle-separated SD orbitals.

Secondly—and arguably more importantly—the CCS approach enables a novel tensor SOP representation of the exact, full N -electron Hamiltonian, that is remarkably efficient and accurate, and that can handle Coulombic singularities with ease—even in a sinc grid-based representation. This is because potential energy functions are not simply evaluated at the grid points. As a consequence, it is possible to place a grid point even directly on a Coulombic singularity, with no particularly damaging numerical repercussions.^{50,57} Likewise—and regardless of the particular CCS basis representation—the Hamiltonian tensor SOP is not some arbitrary numerical approximation to the explicit matrix representation, but is instead a fundamental identity that arises naturally from a CCS analysis of the underlying operators. This is described in detail in the following subsection.

2.2 CCS Tensor SOP Representation of the Hamiltonian

The first-quantized electronic structure Hamiltonian \hat{H} is generally of the form

$$\hat{H} = \sum_{i=1}^N \left(\frac{\hat{p}_{ix}^2}{2m_e} + \frac{\hat{p}_{iy}^2}{2m_e} + \frac{\hat{p}_{iz}^2}{2m_e} \right) + \sum_{i=1}^N V_{\text{ext}}(x_i, y_i, z_i) + \sum_{i<j}^N V_{ee}(x_i, y_i, z_i, x_j, y_j, z_j), \quad (5)$$

where m_e is the mass of the electron. The first sum in Eq. (5) above represents the kinetic energy contribution, which separates by both particle and Cartesian component. The remaining, external (V_{ext}) and pair repulsion (V_{ee}) potential energy terms, respectively, involve three or six coordinates each. These are generally taken to have Coulombic form, although the present method is not necessarily restricted to Hamiltonians of this kind.

Assuming a Coulombic form for the electron pair repulsion contribution, we have

$$V_{ee}(x_i, y_i, z_i, x_j, y_j, z_j) = V_{ee}(s) = 1/s^{1/2}, \quad \text{with} \quad (6)$$

$$s = (x_i - x_j)^2 + (y_i - y_j)^2 + (z_i - z_j)^2.$$

Inverse Laplace transformation then yields the following exact form:

$$\hat{V}_{ee} = \frac{2}{\sqrt{\pi}} \int_0^{\infty} \hat{\gamma}_x(\beta) \hat{\gamma}_y(\beta) \hat{\gamma}_z(\beta) d\beta, \quad \text{where} \quad (7)$$

$$\hat{\gamma}_d(\beta) = \exp[-\beta^2(d_i - d_j)^2] \quad (8)$$

In Eq. (7) above, the individual $\hat{\gamma}_d$ factors in the integrand (e.g., $\hat{\gamma}_x(\beta) = \exp[-\beta^2(x_i - x_j)^2]$) are two-particle operators involving just a single Cartesian component, d . The critical point is that *these factors separate by Cartesian component, and not by particle*. Note that spherical symmetry implies the same form for all of the $\hat{\gamma}_d(\beta)$, and so in practice the d subscript can sometimes be dropped.

A form similar to Eq. (7) has been used previously in electronic structure, in the context of Rys polynomial integrals.⁷⁹ In that context, the component separability of Eq. (7) is exploited in order to simplify the evaluation of Coulomb and exchange integrals—a perennial, if well-established challenge in the electronic structure community. Here, however, the Cartesian component separability of the β integrand is used in an entirely different manner—i.e., to construct a natural tensor SOP representation of the two-electron pair repulsion operator itself. Also, Rys considered only Gaussian basis functions, i.e. not general CCS basis representations of the form of Eq. (3), and certainly not the tensor-SOP reduction [i.e., Eq. (4)].

To convert Eq. (7) above into an explicitly tensor-SOP form, the one-dimensional integral over β is evaluated numerically by quadrature, on a finite and discrete set of quadrature points, β_{λ} . The integral is then effectively replaced with a tensor-product sum of the form

$$\hat{V}_{ee} = \sum_{\lambda=1}^{\Lambda_{ee}} w_{\lambda} \hat{\gamma}_x^{\lambda} \hat{\gamma}_y^{\lambda} \hat{\gamma}_z^{\lambda}, \quad (9)$$

where the w_λ are the quadrature weights [into which the $2/\sqrt{\pi}$ factor from Eq. (7) has also been subsumed]. Remarkably, quadrature schemes with as few as $\Lambda_{ee} = 22$ points have been found that provide accuracies near to machine precision, with substantially smaller Λ_{ee} values required for chemical accuracy (i.e., ~ 1 – 2 millihartree). To our knowledge, no particle-separated tensor-SOP matrix representations of \hat{V}_{ee} provide comparable accuracy with as few terms.^{74,75} That said, recent graphically contracted function (GCF) and all configuration mean energy (ACME) methods show that such dramatic reductions are possible, at least in the multiconfiguration self-consistent field (MC-SCF, including complete active space or CASSCF) and state-averaged contexts.^{76–78}

The individual factors in Eq. (9) are two-particle single-component “potential energy” operators that get represented as single-component matrices as follows (e.g., for x):

$$\begin{aligned} \gamma_{n_x, m_x}^\lambda &= (\beta_\lambda^2 \parallel n_x, m_x) \\ &= \int X_{n_x}^*(x_1, \dots, x_N) e^{-\beta_\lambda^2 (x_i - x_j)^2} X_{m_x}(x_1, \dots, x_N) dx_1 \dots dx_N \end{aligned} \quad (10)$$

For basis functions that are also particle-separated as per Eq. (2) (e.g., plane waves), the integrals in Eq. (10) reduce to two dimensions. Still simpler forms will be considered in Sec. 4, e.g. based on quadrature. Even for optimized, highly correlated CCS basis functions of the Eq. (1) form, the integrals of Eq. (10) can be efficiently integrated numerically—e.g., using a further tensor-SOP decomposition.

In any event, these CCS Coulomb integrals need only be performed once for all time, for a given choice of basis—irrespective of any subsequent electronic structure calculations to which they might be applied. Once the component tensor matrices have been determined as per above, they are used to construct a tensor-SOP representation of the electron pair repulsion contribution to the Hamiltonian operator that requires storage of at most $\Lambda_{ee}(M_x^2 + M_y^2 + M_z^2)$ elements. For plane-wave and other particle-separated CCS basis sets of the Eq. (2) form, only $\Lambda_{ee}L^4$ elements need be stored.

There remain, in the Hamiltonian of Eq. (5), additional contributions from the kinetic energy, and the external potential energy, V_{ext} . If the latter represents Coulombic attraction to nuclei—as is expected to be the most common case—then a CCS tensor SOP form very similar to Eq. (7) may be employed.^{50,57,58} Matrix elements are also defined similarly to Eq. (10). Storage requires $\Lambda_{Ze}(M_x^2 + M_y^2 + M_z^2)$ elements in the most general case—with Λ_{Ze} about as small as Λ_{ee} , despite the fact that the Coulomb interaction is now attractive. For CCS basis sets that are in addition particle-separated [Eq. (2)], the scaling is only $\Lambda_{Ze}L^2$.

On the other hand, it must be recognized that attractive, bare Coulomb potentials tend to generate large errors when plane-wave or sinc basis representations are used. Stated differently, such basis sets represent a very inefficient choice when $V_{\text{ext}}(\vec{r}_i) = -\sum_k Z_k/|\vec{r}_i - \vec{R}_k|$ —for which L values in excess of 100 (or equivalently, $M > 10^6$) may become required in order to attain chemical accuracy, as discussed. Better CCS basis sets, particularly highly correlated ones, will provide much better performance, in terms

of either: (a) greatly reducing the overall basis size N_B needed to achieve a given level of accuracy, or; (b) greatly improving the numerical convergence accuracy for a given N_B . This issue is taken up again in Secs. 2.3 and 3.

It should also be stated that Coulomb potentials are far from the only type for which a Laplace-transformed CCS SOP form can be obtained. In particular, Yukawa and long-range Ewald potentials have also been represented in this fashion.⁵⁸ There are also, of course, external potentials that naturally adhere to the CCS form—such as isotropic harmonic oscillator potentials (i.e. “harmonium”), which have also been considered in this context^{58,66–68} (Sec. 3). Finally, we point out that the Cartesian kinetic energy operator itself [Eq. (5)] is also naturally CCS, and therefore also straightforward and inexpensive to represent in a CCS basis. For further details, please consult [57] and [58], and also Secs. 3 and 4.

The discussion presented in this subsection primarily refers to how the various components of the Hamiltonian matrix of Eq. (5) are represented in tensor-SOP form on a *classical* computer. In particular, use of CCS tensor-SOP representations very dramatically reduces Hamiltonian matrix storage down from the N_B^2 elements that would otherwise have to be stored in an explicit representation. Similarly dramatic savings using a CCS tensor-SOP representation for the wavefunction vector then make it feasible to perform explicit N -electron calculations on a classical computer—to chemical accuracy, even for strongly correlated systems, and for highly excited electronic states, including wavefunctions—at least up to $N = 4$ or so. This is the story, more or less, on the classical computing side.

For the quantum computing implementation, however, things are rather different. Whereas on a quantum computer, qubits are indeed used to represent the wavefunction (albeit explicitly, rather than in tensor-SOP form), the Hamiltonian matrix elements *per se* are *not* stored. Instead, the action of the Hamiltonian on the wavefunction is simulated through the use of appropriate *quantum circuitry*—i.e., a collection of quantum gates—applied to the set of logical qubits used to represent Ψ .

It is worth reflecting on the fundamental differences between the basic QCC framework as described above, and that of traditional linear algebra as implemented on classical computers. In the latter context, a (direct) matrix–vector product is pretty much always implemented numerically in the same way, regardless of the choice of basis used to represent the matrix. Of course, the matrix itself must be stored explicitly, in addition to the vector, and it is in these explicit representations that one encounters variations from one basis set to another. In the QCC context, however, the Hamiltonian matrix is reflected in the form of the quantum circuitry itself—which consequently changes, depending on the choice of basis set. Even for a given basis, there can be many different strategies, all designed to perform the same operation more or less, but using different quantum circuitry.

In any event, the QCC algorithm proposed in this work (Sec. 4) certainly differs from previous quantum circuitry designed to do the same thing. In large measure, this is because it is based on the CCS tensor-SOP representation of \hat{H} , as described in this subsection, but there are some other new wrinkles as well.

2.3 Spin, Permutation Symmetry, and Enforcement of Rigorous Antisymmetry

Due to the Pauli Exclusion Principle, the entire N -electron wavefunction (including spatial and spin components) must be antisymmetric with respect to exchange of any two electrons. More properly, the wavefunction must belong to the totally antisymmetric (A_2) irreducible representation (irrep) of the N -body permutation group, S_N . In the standard particle-separated approach, SDs are used to automatically enforce rigorous antisymmetry of the entire electronic wavefunction. This generally requires that spin states are built into the definition of the single-electron states (spin-orbitals). since our CCS methodology is not based on SDs, some other means must be adopted to enforce rigorous antisymmetry of the entire electronic wavefunction.

Spatial-spin decompositions are fundamental to a wavefunction approach to electronic structure. For this paper, we shall always assume that the entire N -electron wavefunction can be written as the product of an overall spatial wavefunction times an overall spin state. This spatial-spin factorization is legitimate for the Hamiltonians considered here, which do not involve spin explicitly (although the methodology could certainly be generalized to accommodate spin-orbit coupling or other corrections from the Dirac equation). As a consequence, spin never enters into our numerical calculations at all, so that only the spatial part of the electronic wavefunction is ever explicitly represented (e.g., in Sec. 2.1). Each computed numerical energy level would therefore have a 2^N -fold spin degeneracy, were it not for antisymmetry.

Conversely, the spin factor plays a huge rule in determining which spatial wavefunctions can give rise to entire wavefunctions that are antisymmetric. More generally, spin is used to determine the spin degeneracies of the computed electronic states. This is achieved using group theory, as follows. First, for a given permutation group, S_N , the direct-product group (representing the entire wavefunction) is determined. Next, the 2^N -dimensional spin representation is decomposed into its S_N irreps. Based on available spin irreps and degeneracies, and the direct-product table, the corresponding allowed spatial irreps and entire wavefunction degeneracies are determined.

In the two-electron case, this is rather trivial: spatially symmetric (A_1) solutions correspond to spin-singlet (A_2) states, and spatially antisymmetric (A_2) solutions to spin-triplet (A_1) states, as per the standard and familiar rules. Thus, numerically computed (spatial) states for both S_2 irreps are physically realized. For larger N , however, the situation becomes much more complicated, in accord with the corresponding permutation symmetry groups, S_N . For one thing, not all of the S_N irreps are physically realized for $N > 2$. Additionally, there are degenerate irreps that appear, with far less trivial representations in terms of the underlying product basis. The direct-product tables are also decidedly more complicated. Nevertheless, the requisite group theory has been worked out by us, for all cases up to $N \leq 6$.

Let us begin with the S_N irrep decompositions of the 2^N -dimensional spin state representations. These are summarized in Table 1, Column III. Note that A_2 never appears in the spin state irrep decompositions, except for $N = 2$. This implies, e.g.,

Table 1 S_N irrep decompositions of spin state representations for $N \leq 6$ (Column III). This implies allowed (Column IV) and forbidden (Column V) spatial irreps, as indicated, in order to enforce antisymmetry (i.e., A_2 character) on the entire spatial-spin wavefunction.

N	2^N	Spin irrep decomposition	Spatial irreps	
			allowed	forbidden
2	4	$3A_1 \oplus A_2$	A_1, A_2	
3	8	$4A_1 \oplus 2E$	A_2, E	A_1
4	16	$5A_1 \oplus E \oplus 3T_2$	A_2, E, T_1	A_1, T_2
5	32	$6A_1 \oplus 4G_1 \oplus 2H_1$	A_2, G_2, H_2	A_1, G_1, H_1, I
6	64	$7A_1 \oplus 5H_1 \oplus H_2 \oplus 3L_1$	A_2, H_3, H_4, L_2	$A_1, H_1, H_2, L_1, M_1, M_2, S$

that the A_1 spatial states are never physically realized for $N > 2$. More generally, from the direct product tables for S_N , we have ascertained exactly which spatial irreps can give rise to an overall A_2 state. The resultant physically realizable spatial irreps, and also the forbidden irreps, are listed in Columns IV and V, respectively, of Table 1. Note that irreps are labeled as follows. Labels E, T, G, H, etc., refer to irreps that are, respectively, two-, three-, four-, and five-fold degenerate, etc. For groups with more than one irrep of a given degeneracy, subscripts are assigned such that smaller numerical values correspond to more positive character under two-particle exchange.

From Table 1, it is clear that as N increases, an increasingly small fraction of spatial states is allowed by permutation antisymmetry. Roughly speaking, this fraction is found to be 100%, 84%, 58%, 35%, and 18%, for $N = 2-6$, respectively. In order to exploit this situation as much as possible, symmetry adaptation of the CCS basis set may be utilized.^{73,80-83} This improves the efficiency of the calculations, by enabling each irrep to be computed independently of the others. Additionally, we need only perform calculations for those irreps that are physically realizable.

There are two modes in which symmetry adaptation of the basis can be implemented. The first pertains to a general CCS basis of the Eq. (1) form, for which the individual X_{m_x} , Y_{m_y} , and Z_{m_z} factors are themselves S_N -symmetry adapted. This is the eventual goal, i.e. use of a CCS basis for which the individual component-wise factors are fully correlated across all N particles, optimized for the specific application at hand, and symmetry-adapted. More specifically, the single-component, $X_{m_x}(x_1, \dots, x_N)$, etc., basis functions will be obtained as the eigenstates of optimal “effective” component Hamiltonians, \hat{H}_x , etc.,⁸⁴⁻⁸⁶ which themselves are invariant under S_N . The effective component Hamiltonian problems have one-third the dimensionality of the full problem (and can themselves be symmetry-adapted), and are therefore presumed tractable.

Although perhaps a bit counterintuitive at first, the resultant “optimal CCS basis” (OCCSB) functions may be conceptualized as the *component-based analog of the SCF orbitals*. In other words, whereas the SCF molecular orbital structure is what naturally arises when one assumes only separability by particle, the OCCSB is what naturally arises when one assumes only separability by Cartesian component. From a practical computational perspective, the chief advantage in either case is the same: a greatly reduced separable basis size, in comparison, e.g., with a plane wave representation.

We can estimate the basis size reduction as follows. For an explicit plane-wave calculation, the basis size is $N_B = L^{3N}$. A plane-wave basis may be a reasonably good choice for certain applications, but for attractive external Coulomb potentials, it leads to $L \approx 100$ or so, as discussed (Sec. 2.2). For $N = 4$ or more, N_B exceeds one mole in size. For an OCCSB, the basis size is $N_B = M_d^3$. For $N = 4$, we estimate that M_d might be in the range 1000–10000, leading to as few as a “mere” billion total basis functions in all. This is well within reach classically; CCS calculations to date have been performed with from 10^{12} to 10^{18} basis functions^{50,57,58,63}—although basis size *per se* is not the only factor governing overall cost of the calculation. Further details are provided in an upcoming publication, with Sec. 3 of this paper also providing some new and compelling numerical evidence, in the context of the harmonium calculations.

In any event, for any CCS basis that respects component-wise S_3 symmetry (i.e., whether the OCCSB or not), symmetry adaptation for the final $3N$ -dimensional basis of Eq. (1) is straightforward to manage. In effect, each triple-Cartesian product implied by Eq. (1) has an S_N character decomposition that can be determined using two applications of the S_N direct-product table. In practice then, one simply gathers together the triple-product basis functions for a given (physically allowed) irrep, and uses just those basis functions to construct a symmetry-adapted block of the Hamiltonian matrix.

The second mode of symmetry adaptation applies in cases where the $X_{m_x}(x_1, \dots, x_N)$, etc., functions are *not* themselves symmetry-adapted. This is necessarily the case if the basis functions are also particle-separated, as in Eq. (2). In such cases, the basis functions naturally partition into equivalence classes for which the N individual m_{id} indices are identical, apart from permutations. It is then possible to create symmetry-adapted linear combinations from each such equivalence class, as follows:^{73,80–83} (a) using the S_N character table, construct the representation of the projection operator for each irrep, in the small set of basis functions in a given equivalence class; (b) apply each projection operator to each product basis function in turn, to construct the symmetry-adapted linear combinations.

The above procedure has been applied for the $N = 3$ and $N = 4$ applications presented in Sec. 3, which represent the first $N > 2$ CCS calculations ever performed. Although there are a number of possible scenarios (reminiscent of quantum statistics) a simple example will serve to clarify the procedure. Consider a set of $N = 3$ particle-separated basis functions of the Eq. (2) form, for which two of the three indices, m_{1x} , m_{2x} , and m_{3x} have the same value m , and the third has a different value $n \neq m$. This defines an equivalence class of three orthogonal basis functions, i.e.

$$\phi_n^x(x_1)\phi_m^x(x_2)\phi_m^x(x_3) = \langle x_1x_2x_3 | nmm \rangle$$

$$\phi_m^x(x_1)\phi_n^x(x_2)\phi_m^x(x_3) = \langle x_1x_2x_3 | mnm \rangle$$

$$\phi_m^x(x_1)\phi_m^x(x_2)\phi_n^x(x_3) = \langle x_1x_2x_3 | mmm \rangle$$

Construction and application of the irrep projection operators then results in one (unnormalized) linear combination with A_1

character, zero combinations with A_2 character, and two combinations forming an E pair, as follows:

$$A_1 : \quad |nmm\rangle + |mnm\rangle + |mmm\rangle \quad (11)$$

$$E : \quad |nmm\rangle + |mnm\rangle - 2|mnm\rangle, \quad (12)$$

$$|nmm\rangle - |mnm\rangle \quad (13)$$

On reflection, the permutation symmetry adaptation schemes used in the CCS context, as described above, are certainly much more complicated than the simple and familiar SD “work horse.” However, they are also much more flexible, as they can be applied to any possible combination of spin and spatial states, and moreover, need not be restricted to overall A_2 symmetry character. This last point is extremely important, *vis-à-vis* generalizing the CCS method for the combined electron-nuclear motion quantum many-body problem, wherein electrons and nuclei (be they fermions or bosons, identical or not) are treated on an equal footing. Such applications present a rich, group theoretical structure that cannot be fully addressed with SDs alone. They are, however, easily amenable to the CCS symmetry adaptation tools as laid out in this subsection—thereby addressing point (c) from Sec. 1.

We conclude this subsection with a brief discussion of numerical contamination. On a classical computer, it is well-known that numerical roundoff error can introduce a tiny contribution from the wrong symmetry character into the wavefunction. Moreover, repeated applications, e.g. of the Hamiltonian acting on the wavefunction, can magnify this error exponentially.^{87,88} There is, however, a simple remedy for this problem as well; periodically, the projection operator for the desired irrep should be applied to the current wavefunction, to ensure its purity.

Intriguingly, the situation on a quantum computer is quite different. There are, first of all, various methods that have already been devised for imposing rigorous antisymmetry on first-quantized qubit representations of the initial electronic wavefunction, analogous to the procedures described above.^{8,35,89} Whereas the original methods were admittedly quite slow,⁸ a recent first-quantized technique has been shown to be exponentially faster.⁸⁹ In particular, the gate complexity scales as $O(N \log N \log L)$, and is trivial compared to other quantum computational costs (e.g., for QPE).

There is also the issue of error propagation. As in the classical computing case, small symmetry errors are to be expected. Interestingly, however, a recent, rigorous error bound characterization³⁵ found that these errors do *not* grow exponentially with repeated applications. This is a quite important result, evidently due to the fact that all operations performed on a quantum computer are rigorously unitary—unlike the analogous operations on a classical computer. It is also quite fortuitous, as the implementation of projection operators that would otherwise be required to purify the wavefunction might pose a difficulty on a quantum computer, because projections are necessarily *non-unitary* operations.

3 Results: Classical Computing Benchmarks

The classical CCS algorithm has been implemented in our computer code, *Andromeda*, and applied to several small benchmark applications, with $N = 2, 3$, and 4 explicit electrons.^{50,57,58,63} In every case to date, a plane-wave or sinc basis representation was used. Results for selected earlier and preliminary work are summarized in Sec. 3.1. In Sec. 3.2, we present results for the “harmonium” system (i.e., with harmonic external field V_{ext}), including earlier $N = 2$ calculations,⁵⁸ together with new results for $N = 4$. Other prior or preliminary results, e.g. for long-range Ewald potentials,⁵⁸ for the H_2 ⁵⁷ and H_3^+ electronic structure problems, and for the H_2 and H_2^+ combined electron-nuclear motion problems,^{64,65} will not be discussed further here.

Collectively, the above model calculations are useful in their own right, but also in terms of what they reveal about prospects for the classical CCS methodology, once optimized OCCSB basis sets are employed instead of plane waves. The model calculations are also quite useful as benchmarks for first-quantized QCC calculations—providing more accurate estimates for the required number of qubits, for example, than the methods that have been relied upon in the past.

First, however, we provide a very brief overview of the classical CCS algorithm, as it is currently implemented in *Andromeda*. For a much more detailed exposition, please consult the references.^{50,57,58} To begin with, the CCS tensor-SOP representations for both the wavefunction vector and the Hamiltonian matrix have already been specified, in Eqs. (4) and (9), respectively. Insofar as the algorithm is concerned, the main operation is a block Krylov subspace procedure, similar to Lanczos.⁹⁰ This requires a sequence of matrix–vector products with the Hamiltonian. Since both matrix and vector are tensor SOPs, the operation is fast. On the other hand, the tensor-SOP rank—or number of terms, Λ , in the Eq. (4) sum—increases rapidly with each successive matrix–vector product. To curb this growth in Λ , the alternating least squares (ALS) approach of Beylkin and coworkers is used.⁷¹

3.1 Summary of previous classical CCS results

Li Atom:⁵⁷ The simplest benchmark calculation possible is the hydrogen atom ($N = 1$). In (Ref. [57]) we computed the ground state energy of the non-relativistic H atom to an accuracy of ~ 0.3 millihartree (i.e., much better than chemical accuracy). A bare Coulomb potential was used with a plane-wave basis, which constitutes a “worst-case” choice, as discussed. A single-coordinate basis size of $L = 81$ was required, corresponding to a second-order full-CI matrix diagonalization calculation with $M = 531,441$ orbitals and $N_B = 531,441$ SDs.

He Atom:⁵⁷ In the original study of Ref. [57], an explicit $N = 2$ calculation of the He atom was also performed, again with bare Coulomb potentials and a plane-wave basis. The greater $Z = 2$ attraction of the He nucleus as compared with H necessitates a somewhat finer grid. Moreover, energy excitation and partial screening demand larger coordinate ranges. Consequently, $L = 101$ is now required to converge the lowest-lying dozen or

so electronic states to chemical accuracy. This corresponds to a second-order full-CI matrix diagonalization calculation with $M = 1,030,301$ orbitals and $N_B \approx 1.0615 \cdot 10^{12}$ SDs. Note that we are able to obtain the excited electronic energies (and wavefunctions) without expending any additional numerical effort beyond that required to obtain the ground state.

Finally, in more recent (unpublished) work, the plane wave basis was supplemented with additional Gaussians to better handle the cusp region. This enabled reduction of numerical convergence error to tens of *microhartrees*.

Li Atom: A first-quantized plane-wave calculation of the Li atom ($N = 3$) ground state energy has been touted as an important QCC benchmark.³⁵ The main reasons are that: (a) the required number of logical qubits has been estimated to be at least 100, and may therefore not be very far beyond present-day limits of quantum hardware, and; (b) the classical calculation is believed to be intractable. Conversely, if the above Li atom calculation is actually possible on a classical computer, then this finding would be quite significant, because it would provide an important first-quantized QCC benchmark, while simultaneously pushing back the threshold for “quantum supremacy.”

Using our classical CCS code *Andromeda*, we have obtained preliminary results for the Li atom—again, treating all electrons explicitly, and using bare Coulomb potentials and a plane-wave basis. Our preliminary results suggest not only that a classical calculation is possible, but also that a chemically accurate QCC calculation (performed using exact γ matrices; see Sec. 4.3) should require only ~ 60 logical qubits ($3Nn = 63$, with $N = 3$ and $n = 7$). This places the Li atom application within much closer reach of present-day quantum hardware than might have been imagined. On the other hand, our assertion is not yet fully confirmed, as it is based on an $L = 101$ ($M = 1,030,301$, $N_B = 1.0937 \cdot 10^{18}$) classical calculation that is not fully completed. In particular, the computed ground state energy is not yet Krylov-converged.

In any event, there is an independent indication that the basis set convergence itself is sufficient to achieve at least near-chemical accuracy. More specifically, *Andromeda* has the capability to compute the total probability of a computed wavefunction along each of the $6N$ position coordinate edges (i.e., minimum and maximum d_i grid values), and also each of the $6N$ momentum space edges. According to this metric, the largest position-edge probability for the ground state wavefunction is $9.0 \cdot 10^{-7}$, whereas the largest momentum-edge probability is $2.4 \cdot 10^{-5}$. These values are on a par with similar basis-set converged calculations for He and H as described above.

Correlated Electron Gas (CEG):⁶³ The above examples clearly demonstrate that plane waves are not well suited for systems with attractive bare Coulomb potentials. Even so, we have been able to perform explicit all-electron calculations of this kind for systems with up to $N = 3$ and $N_B = 10^{18}$. How much further could we scale up in N , if a more “competitive” basis such as OCCSB were employed? Short of actually performing such calculations, the next best thing would be to find systems for which the plane-wave basis itself might be nearly optimal. For this purpose, the best application is probably the “correlated electron gas” system—i.e., with $V_{\text{ext}} = 0$, periodic boundary conditions, and a fixed number

of electrons per unit cell (in contrast to the uniform electron gas or “jellium” model^{60–62}).

Using Ewald summations, we are computing exchange-correlation energies for the correlated electron gas system with $N = 2, 3$, and 4 explicit electrons, for both spin-restricted and spin-unrestricted cases. An extremely broad range of Wigner-Seitz radii is being considered, ranging from metallic to Wigner crystal regimes where correlation effects dominate. This project is still ongoing.⁶³ However, the best indication is that $L = 11$ suffices for most Wigner-Seitz radius values. As anticipated, this represents a very dramatic reduction in basis size—i.e. down to $M = 1331$ or $N_B = 3.138 \cdot 10^{12}$ (for $N = 4$). Put another way, such small L values suggest that explicit classical CCS calculations up to $N = 6$ may be possible.

3.2 Harmonium

The Hamiltonian for the harmonium system is identical to that of the standard electronic structure form of Eq. (5), except that the attractive bare Coulomb external potential is replaced with the following confining harmonic field:^{58,66–68}

$$V_{\text{ext}}(x_i, y_i, z_i) = \frac{\omega^2}{2} (x_i^2 + y_i^2 + z_i^2) \quad (14)$$

As a technical matter, too, we consider harmonium with a Yukawa, rather than Coulomb, form for the pair repulsion potential:

$$V_{ee}(\vec{r}_i, \vec{r}_j) = e^{-\gamma|\vec{r}_i - \vec{r}_j|} / |\vec{r}_i - \vec{r}_j| \quad (15)$$

One of the remarkable features of harmonium—or the “Hooke atom,” as it is also called—is that (nearly) analytical solutions exist for the $N = 2$ case, despite the coupling implied by the pair repulsion contribution. This makes it possible to compare numerically computed results directly with “exact” values, thus offering an excellent opportunity to benchmark new methods.

For our purposes, we are also interested in harmonium as an “intermediate” test case, lying in between the pathological Coulomb V_{ext} form of the atomic models, and the $V_{\text{ext}} = 0$ form of the correlated electron gas model (Sec. 3.1). In particular, we expect that the plane-wave basis—though not an especially good choice for harmonium—will nevertheless perform far better here than for bare Coulomb potentials. Of course, there are many contexts in electronic structure in which the bare Coulomb interaction is replaced with “milder” forms—e.g., screened potentials (including SCF), effective core potentials, “softened” Coulomb potentials, etc.

In Ref.^[58] we used *Andromeda* to perform a classical CCS calculation of the 20 lowest-lying energy eigenstates (i.e. energy levels and wavefunctions) for the $N = 2$ harmonium system with $\omega = 1/2$ and $\gamma = 1$ (in atomic units). This parameter choice guarantees “non-trivial” behavior—with neither the external confining field nor the interparticle repulsion contribution dominating. By comparing with the exact analytical results, we were able to confirm an overall numerical convergence of all states to better than a few tens of *microhartrees*. Moreover, this was achieved using a *much* smaller basis than in the atomic examples of Sec. 3.1—i.e., $L = 33$ (or $M = 35,937$, $N_B = 1.2915 \cdot 10^{12}$). For chemical accuracy,

the L value could be reduced by about another factor of two.

For the present study, we have extended the above harmonium calculations out to $N = 4$, using the same ω and γ values. More specifically, we have computed the lowest-lying 15 states belonging to the A_1 and T_2 irreps, with the goal of achieving chemical accuracy. The results, together with Krylov convergence errors, are presented in Table 2. By this measure, near chemical accuracy is indeed achieved (rms error = 1.8 millihartree), using a single-coordinate basis size of only $L = 17$ (i.e., as predicted by the $N = 2$ calculation). This corresponds to $M = 4913$ or $N_B \approx 5.8262 \cdot 10^{14}$.

For the $N = 4$ harmonium ground state energy, the Krylov convergence error is only ~ 0.4 millihartree. For this state, we have also used *Andromeda* to compute edge probabilities (as for the Li atom in Sec. 3.1 above). The largest position-edge probability is found to be only $2.43 \cdot 10^{-7}$; the largest momentum-edge probability is only $1.74 \cdot 10^{-9}$. These values imply a very small basis set truncation error—which, in any event, is likely to be much smaller than other sources of numerical error for this calculation.

Table 2 Fifteen lowest-lying energies for the $N = 4$ harmonium system (atomic units), as computed using the *Andromeda* classical CCS code, for the A_1 and T_2 irreps (Column III). Numerical convergence errors (Column IV) are taken relative to the previous Krylov iteration. S_4 irrep labels (Column II) refer to the spatial part of the wavefunction only.

State index	Spatial irrep	Energy	Error
1	A_1	3.6341	-0.0004
2	A_1	3.9406	-0.0010
3	A_1	3.9572	-0.0025
4	A_1	3.9663	-0.0017
5	T_2	4.1045	-0.0007
6	T_2	4.1288	-0.0010
7	T_2	4.1349	-0.0021
8	A_1	4.3455	-0.0029
9	A_1	4.3668	-0.0048
10	A_1	4.4304	-0.0025
11	A_1	4.4540	-0.0036
12	A_1	4.4799	-0.0036
13	T_2	4.4945	-0.0016
14	T_2	4.4999	-0.0020
15	T_2	4.5057	-0.0021

4 Results: Quantum Computing Implementation

As discussed, in “first quantized” QCC,^{8–15,20–23,26,35} the wavefunction is represented explicitly, as a function over the entire $3N$ -dimensional configuration space of electron positions. A set of logical qubits is used for this purpose—e.g., to represent the value of the wavefunction at each of a set of uniformly-spaced sinc grid points, forming a $3N$ -dimensional lattice. An initial wavefunction is generated, and then manipulated through specialized quantum circuitry, in order to simulate the action of the Hamiltonian. Eventually, through many such manipulations, the time-dependent evolution of the initial wavefunction is simulated—or alternatively, the energy eigenstates are computed.

For the types of quantum chemistry applications for which QCC methods can currently be implemented, using today’s quantum (or hybrid quantum/classical) computers, the second-quantized methods have the upper hand. This is because such calculations use the standard simplifying approximations, wherein the num-

ber of orbitals, M , and/or the number of SDs, $\binom{M}{N}$, is greatly reduced from the CBS-limit and/or full-CI values. This yields a greatly simplified calculation requiring exponentially less computational effort than a fully converged calculation—which is generally not currently feasible on either classical or quantum computers except for very small systems. Even so, the list of such simple applications that have actually been realized using second-quantized QCC—which includes, e.g. crude ground state calculations for the H_2 molecule and other two-electron systems^{29,35}—still remains short and unimpressive in comparison with state-of-the-art quantum chemistry on classical computers.^{76–78}

Returning to first-quantized QCC, the primary feature here is that the cost to store the wavefunction, in terms of the required number of logical qubits, scales only *linearly* with N . Our first task in this section, then, is to estimate the number of logical qubits required—even if it is larger than what can be accommodated on current quantum hardware. Our second task shall be to explain the quantum circuitry used to implement the above-referenced Hamiltonian-based manipulations of the wavefunction, in precise detail. This we shall do both for the “standard” or canonical Trotter approach, and also for our alternate CCS-based Trotter implementation, to which the former will be compared.

4.1 Explicit Quantum Representation of the Wavefunction

Note that both tasks above depend intimately on the choice of basis set. For convenience and simplicity, we shall throughout this section presume either a plane-wave, or a sinc (plane-wave dual), basis representation—with the latter related to the former via an inverse Fourier transform. Note that both basis representations conform to Eq. (2). Let $|\psi\rangle$ denote the $3N$ -dimensional numerical wavefunction vector, whose individual components are denoted

$$\Psi_{m_x m_y m_z} = \Psi_{m_{1x}, \dots, m_{Nx}, m_{1y}, \dots, m_{Ny}, m_{1z}, \dots, m_{Nz}} \quad (16)$$

from Eqs. (2) and (3). There are clearly L^{3N} such components in all.

The total number of logical qubits needed to represent the entire $|\psi\rangle$ is thus $3Nn$, with $L = 2^n$. Thus, for $L \approx 100$, we can expect $n \approx 7$. Note that for each of the $3N$ coordinates, d_i , there is a specific set of n qubits, used to represent the L corresponding one-dimensional basis functions, $\phi_{m_{id}}^d(x_i)$. We therefore associate each such bundle of n qubits with the coordinate d_i , but, also with the part of the wavefunction associated with that coordinate, which we call $|\psi_{id}\rangle$. Note that the concept of $|\psi_{id}\rangle$ has meaning in quantum computing, *even when* $|\psi\rangle$ itself is not separable *per se*.

In quantum computing circuit diagrams, individual qubits are traditionally represented as horizontal “wires”. These flow from left to right, encountering various quantum gates along the way that alter the qubit states—and thereby, also, the corresponding $|\psi\rangle$. In addition to the logical qubits representing $|\psi\rangle$, various “ancilla” or workspace qubits are also often relied upon, to be used at various stages throughout the quantum computation. These are often used to get around unitarity restrictions—although here, the ancilla qubits generally represent function outputs. Ancilla qubits are typically presumed to be in an initial (and often final) state of “zero”, which we denote as $|0\rangle$.

Some additional quantum circuit conventions that we adopt here are described next. Since for each dimensional set, the number of qubits, n , is fixed—and since there is no reason to consider subdividing below the level of a single coordinate—in all of the quantum circuit diagrams presented here, we treat connections involving $|\psi_{id}\rangle$ as if they were *single-qubit wires*, rather than bundles. As additional notation, let $|\psi_i\rangle$ represent the part of $|\psi\rangle$ associated with particle i , spanning all three Cartesian coordinates, x_i , y_i , and z_i . Likewise, $|\psi_{ij}\rangle$ includes all Cartesian coordinates for particles i and j , whereas $|\psi_{ijd}\rangle$ includes just the two d 'th components—e.g., $|\psi_{12x}\rangle$, associated with x_1 and x_2 . Also, whereas $|\psi\rangle$ refers to the wavefunction in the sinc representation, the corresponding Fourier or plane-wave representation is denoted $|\tilde{\psi}\rangle$.

Finally, the usual “slash” notation will be used for ancilla qubit bundles, representing function outputs. To achieve chemical accuracy, each such bundle will typically require 15–20 qubits, minimum. Going forward, we choose model CCS QCC parameters based on the benchmark Li atom calculation as described in Sec. 3.1. As a conservative choice, $n = 7$ qubits per coordinate, and $3n = 21$ qubits per ancilla bundle, provides an energy function resolution (on the overall energy scale of the Li atom problem) of around $4.0 \cdot 10^{-6}$ hartree—which is well beyond chemical accuracy. Note also that the range of all coordinates in our Li atom calculation is given by the maximum value, $x_{\max} = 7.6$ bohr. In Sec. 4.2, we use these values to estimate the corresponding n value that would be required using the canonical Trotter method.

4.2 Quantum Circuitry: Canonical Trotter Method

Next we address the second task above, i.e. describing the quantum circuitry necessary to implement the requisite Hamiltonian manipulations of $|\psi\rangle$. For both time-independent and time-dependent QCC applications, one must apply unitary time evolution of the form $|\psi(t)\rangle = \hat{U}(t)|\psi(0)\rangle$,^{12,13,35} where $|\psi(0)\rangle$ is the initial wavefunction. In the time-dependent context, this directly propagates the wavefunction, as desired. In the time-independent context, quantum eigensolvers such as quantum phase estimation (QPE)^{11,12,29,30,35} are used to obtain the ground eigenstate (and in some cases, excited eigenstates); however, this too requires unitary time evolution of the above form.^{11,12,29,30,35}

The specific form of the time-evolution operator is $\hat{U}(t) = \exp[-(i/\hbar)\hat{H}t]$, where t is the final time, and \hbar is the reduced Planck's constant (taken to be unity in all that follows). In the canonical Trotter method, this is implemented via repeated applications of $\hat{U}(\varepsilon)$, where ε is a sufficiently small time step such that the individual contributions from Eq. (5) can be treated separately. In other words,

$$\begin{aligned} \hat{U}(\varepsilon) \approx & \dots \exp[-i\varepsilon \hat{V}_{ee}(x_1, y_1, z_1, x_2, y_2, z_2)] \times \\ & \dots \exp[-i\varepsilon \hat{V}_{\text{ext}}(x_1, y_1, z_1)] \times \\ & \dots \exp\left[-i\varepsilon \frac{\hat{p}_{1z}^2}{2m_e}\right] \exp\left[-i\varepsilon \frac{\hat{p}_{1y}^2}{2m_e}\right] \exp\left[-i\varepsilon \frac{\hat{p}_{1x}^2}{2m_e}\right], \end{aligned} \quad (17)$$

an approximation known as “Trotterization,” or the Lie-Trotter-

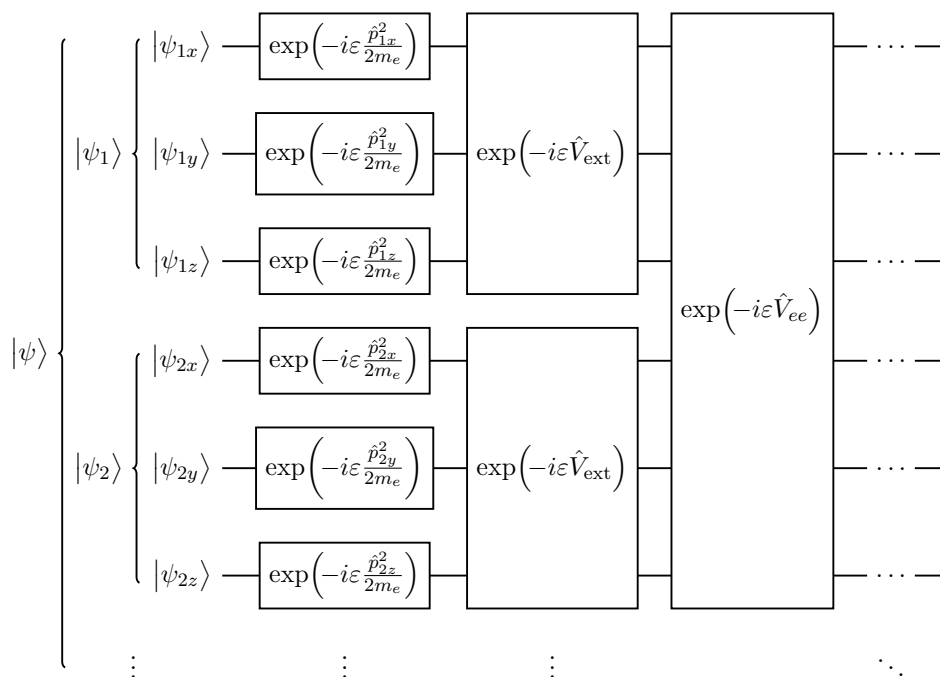


Fig. 1 Overview of quantum circuit to implement unitary short time evolution, $\hat{U}(\epsilon)|\psi\rangle$, via Trotterization, on a quantum computer. This structure is used in both the canonical and CCS Trotter quantum circuitry.

Suzuki decomposition.^{9,12,18,28,35,69} An overview of the quantum circuit implementation of $\hat{U}(\epsilon)|\psi\rangle$, based on Eq. (17), is presented in Fig. 1. Note that the associated ancilla bits, needed to carry out the individual operations in practice, are not indicated in this figure.

We next turn to the canonical Trotter implementation of the various Hamiltonian component contributions in Eq. (17) and Fig. 1. To begin, we note that it is easiest to implement matrix-vector products on a quantum computer, if the matrix is diagonal. Then, the additional condition of unitarity implies that each $|\psi\rangle$ component is simply multiplied by some phase shift. However, we further note that, due to basis set truncation error, the sinc basis representation is only an *approximate* position representation. Thus, in reality, an exact sinc-function representation of the potential energy contributions in Eq. (17) gives rise to matrices that are only *nearly* diagonal. More specifically, we find that the sinc functions themselves are not true Dirac delta functions, but rather, narrowly peaked functions centered around a uniformly-distributed set of discrete grid points, known as the “sinc discrete variable representation” (sinc DVR) grid points.^{44–49}

We are therefore led to a natural, diagonal, grid-based *approximation* to the true potential matrices, obtained by simply evaluating the potential function at the individual sinc DVR grid points, taking these values to comprise the diagonal matrix elements, and then setting the off-diagonal elements to zero.⁴⁸ Note that this procedure introduces new “quadrature error,” above and beyond the basis set truncation error already present.^{44–49} Coulomb potentials—being both singular and long-range—present a “worst-case scenario” in terms of sinc DVR quadrature error. For example, one must avoid placing sinc DVR grid points directly on Coulombic singularities, or the sinc DVR

matrix elements become infinite! On the other hand, the basis set truncation errors associated with sinc or plane-wave representations of Coulomb potentials also present a worst-case scenario, as discussed previously.

As an aside, we can now return to our estimation of the value of n needed to implement the canonical Trotter method for the model Li atom calculation, as described at the end of Sec. 4.1. Given that the core electrons are unscreened near the origin, we can use the $Z = 3$ hydrogenic ground state orbital, $|\psi_{1s}\rangle$, to determine how well the sinc DVR above estimates the analytical expectation value, $\langle\psi_{1s}|V_{\text{ext}}|\psi_{1s}\rangle = -9$ hartree. The best sinc DVR performance is realized using a “half-integer” grid placement, which places the origin exactly half-way between two adjacent grid points. The procedure, then, is to reduce the grid spacing until the numerical quadrature error in the expectation value calculation is reduced down to the energy threshold identified at the end of Sec. 4.1 for the corresponding CCS calculation. Having performed this calculation numerically, we find that the resultant number of sinc DVR grid points in each $[-x_{\text{max}}, x_{\text{max}}]$ coordinate interval becomes $L \approx 24,000$, corresponding to $n = \log_2 L = 14.6$. Even if we relax the error threshold to the level of chemical accuracy, these numbers become $L \approx 1014$ and $n \approx 10.0$.

Returning to a discussion of quantum circuitry, it is in the fashion described above that the potential energy contributions in Eq. (17) are implemented in the canonical Trotter approach—i.e., as phase shifts obtained from potential energy evaluation at the sinc DVR grid points. Put another way, since the potential energy matrices are diagonal in the sinc DVR, their contribution to the time evolution can be implemented using ordinary function evaluation—a standard operation for quantum computers.^{8,9,12,19,33,37} Note that each such function evaluation involves

only a subset of coordinates—and therefore only a subset of qubits, as indicated in Fig. 1. Specifically, each external (V_{ext}) or pair repulsion (V_{ee}) potential energy term involves three or six coordinates, respectively.

Based on the above description in terms of sinc DVRs, the quantum circuit used to implement $\exp(-i\varepsilon\hat{V}_{ee})|\psi_{12}\rangle$ is given in Fig. 2. A bundle of ancilla qubits (lowest wire) is used to represent the value of the function, $V_{12} = V_{ee}(x_1, y_1, z_1, x_2, y_2, z_2)$, which becomes the output of the first gate encountered—i.e., the V_{ee} gate indicated near the lower-left corner. Note that this gate also receives input from six explicit coordinates or sets of qubits—i.e., $6n$ qubits in all, in addition to the ancilla bundle. These act as “control qubits,” associated with specific sinc DVR grid points, whose purpose is to determine the associated function output value. Once the latter value is determined, it is then directed to the second gate, where it is used to effect a phase shift. Note that as a matter of notation, we use $e^{-i\varepsilon V_{12}}$ to refer to the phase shift gate in the quantum circuit diagram, whereas $\exp(-i\varepsilon\hat{V}_{ee})$ refers to the corresponding quantum operator. Finally, a second V_{ee} function evaluation is applied, in order to “reset” the ancilla qubits.

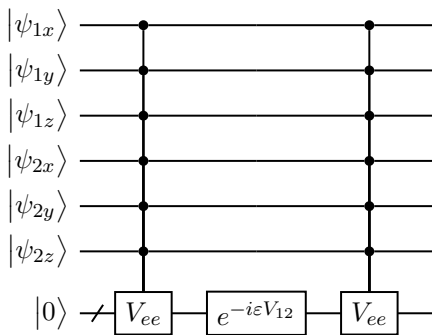


Fig. 2 Canonical quantum circuit to implement $\exp(-i\varepsilon\hat{V}_{ee})|\psi_{12}\rangle$ on a quantum computer. The function evaluation, $V_{12} = V_{ee}(x_1, y_1, z_1, x_2, y_2, z_2)$, involves six explicit coordinates and sets of qubits, and includes an inverse square-root evaluation.

The first gate in Fig. 2 represents one fairly standard way to evaluate functions on quantum computers—which is really based on reversible classical computing. The function evaluation gate (in this case V_{ee}) is a controlled, reversible permutation operation that acts as follows. If the control qubits are all in definite, unsuperposed states, so that they represent one specific point [in this case, $(x_1, y_1, z_1, x_2, y_2, z_2)$], then the function gate permutes the unsuperposed input constant state 0 into the unsuperposed desired function output constant [in this case $V_{ee}(x_1, y_1, z_1, x_2, y_2, z_2)$]. In this manner, unitarity is achieved—since the permutation operation is invertible.

Canonical implementation of the V_{ee} function evaluation gate is complex. Not only does this gate receive input from many control and ancilla qubits, but the standard pair repulsion function itself is also highly correlated, and involves Coulombic singularities that must be carefully avoided, as discussed. In addition to multiplications and additions, which are fairly straightforward to implement (even error-corrected) on a quantum computer,^{91–103} the V_{ee} function also requires evaluation of an inverse square-root, which at present is extremely costly if reasonable accuracy

is required.^{56,95,104} All of this implies a large circuit complexity—rendering the $\exp(-i\varepsilon\hat{V}_{ee})$ operation the computational bottleneck of the entire canonical Trotter approach (as indeed, is also generally the case for classical algorithms).

For $\exp(-i\varepsilon\hat{V}_{\text{ext}})$, a similar, but simpler circuit than Fig. 2 may be used, for which there are only three explicit coordinates and thus three sets of control qubits, associated with a single particle. However, this still represents greater complexity than is desired. As a design goal, we seek to reduce the complexity of the calculation down to a few operations involving no more than one or two qubit sets:

1. operations that involve a *change of representation* (e.g., QFT) should be efficiently reducible to a *single* qubit set.
2. operations that do *not* involve a change of representation should be efficiently reducible to *two* qubit sets.

It remains to consider the kinetic energy contributions to Eq. (17). From Fig. 1, we observe that each such contribution satisfies Condition 1. above; only a single qubit set is involved. This is, of course, because of the fact that the kinetic energy is separable by both particle and Cartesian component. On the other hand, the $\hat{p}_{id}^2/(2m_e)$ contributions are decidedly *not* diagonal in the sinc representation. A Fourier transform is thus required—to transform from the sinc to the plane wave representations, in terms of which the matrix representation of $\hat{p}_{id}^2/(2m_e)$ becomes diagonal. This is performed using the standard quantum Fourier transform (QFT) algorithm,^{11,12,70} denoted “ FT ” in the quantum circuit diagrams. Specifically, FT is applied to $|\psi_{id}\rangle$, which thus becomes $|\tilde{\psi}_{id}\rangle$. Then, the $e^{-i\varepsilon\hat{p}_{id}^2/2m_e}$ phase shift can be implemented, in similar fashion to Fig. 2. The quantum circuit implementation for this entire $\exp[-i\varepsilon\frac{\hat{p}_{ix}^2}{2m_e}]|\psi_{1x}\rangle$ operation is indicated in Fig. 3, for $i = 1$ and $d = x$.

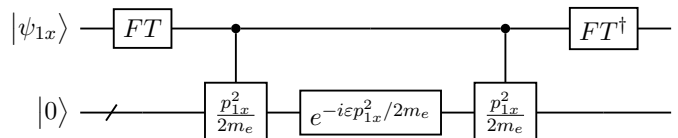


Fig. 3 Quantum circuit to implement $\exp[-i\varepsilon\frac{\hat{p}_{ix}^2}{2m_e}]|\psi_{1x}\rangle$ on a quantum computer. The function evaluation involves just a single coordinate (the momentum p_{1x}), and hence just a single qubit set. This circuit is used in both the canonical and CCS Trotter quantum circuitry.

4.3 Quantum Circuitry: CCS Trotter Method

For the CCS implementation proposed here, much of the canonical Trotter quantum circuitry can be retained. In particular, from a high-level perspective, the overview as presented in Fig. 1 applies equally well to both the canonical and CCS Trotter quantum strategies. Our CCS implementation as presented here is thus also a Trotterized approach. Furthermore, action of the kinetic energy operator is still implemented exactly as in Fig. 3, as it adheres to our “design philosophy” as described in Sec. 4.2.

On the other hand, the CCS implementations for $\exp(-i\varepsilon\hat{V}_{\text{ext}})$, and for the bottleneck $\exp(-i\varepsilon\hat{V}_{ee})$ operation, are very different

from the canonical approach. Specifically, we pursue a quantum circuit implementation in keeping with the CCS tensor-SOP decomposition described in Sec. 2.2. For brevity, we focus the discussion that follows on the more challenging case of implementing $\exp(-i\varepsilon\hat{V}_{ee})$, although similar procedures can also be applied for $\exp(-i\varepsilon\hat{V}_{\text{ext}})$.

From the CCS tensor-SOP form of Eq. (9), it is clear that a natural quantum circuit implementation for $\exp(-i\varepsilon\hat{V}_{ee})|\psi_{12}\rangle$ should take the form presented in Fig. 4. In comparing with the canonical quantum circuit of Fig. 2, we see that the two implementations are completely different. The CCS version would appear to offer many advantages. In particular, the six-dimensional function calls are replaced with $\exp(-i\varepsilon\hat{\gamma}_d^\lambda)|\psi_{12d}\rangle$ operations involving just *two* coordinates (e.g. x_1 and x_2)—thereby satisfying design Condition 2. above. Moreover, the $\hat{\gamma}_d^\lambda$ functions themselves are Gaussians, with very smooth behavior and a restricted, well-defined range.

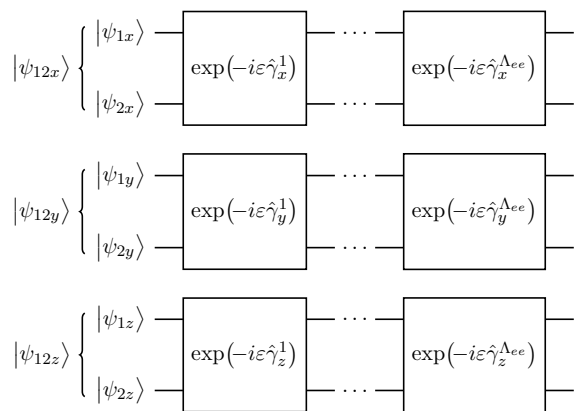


Fig. 4 CCS quantum circuit to implement $\exp(-i\varepsilon\hat{V}_{ee})|\psi_{12}\rangle$ on a quantum computer, based on Eq. (9). The six-dimensional V_{ee} function gate of Fig. 2 is now replaced with two-dimensional function gates, which separate by Cartesian component. The two-particle wavefunction contribution $|\psi_{12}\rangle$ decomposes naturally into $|\psi_{12x}\rangle$, $|\psi_{12y}\rangle$, and $|\psi_{12z}\rangle$ components.

As implied above, the $\hat{\gamma}_d^\lambda$ matrix representations are diagonal in the sinc DVR, and thus amenable to a straightforward quantum circuit implementation—i.e., essentially a two-dimensional version of Fig. 2. The specific quantum circuit used to implement $\exp(-i\varepsilon\hat{\gamma}_d^\lambda)|\psi_{12d}\rangle$ in the sinc DVR is presented in Fig. 5. Note that a similar quantum circuit may be employed for the CCS tensor-SOP components of V_{ext} , except that only a single coordinate or set of control qubits is needed.

Diagonal sinc DVR $\hat{\gamma}_d^\lambda$ matrices certainly present one reasonable avenue for QCC implementation of the CCS approach. Their Gaussian form, moreover, implies that far fewer grid points would be needed to represent \hat{V}_{ee} (to the same level of accuracy) than what was estimated in Sec. 4.2 to be needed for the canonical approach. On the other hand, a sinc DVR calculation still does introduce some quadrature error, which does not exist in the *classical* CCS implementation—e.g., as was used to generate the results of Sec. 3. For this reason, it might be less efficient, in terms of basis size, than the corresponding classical calculation. That said, insofar as factors determining the necessary basis size is concerned, \hat{V}_{ext} is *much* more important than \hat{V}_{ee} , if bare Coulomb potentials are used. Consequently, it is not so clear how much worse

this CCS form of quadrature error would actually make things, in practice.

Nevertheless, we maintain that it is worth the effort to try to develop alternate QCC implementations that use *exact* sinc $\hat{\gamma}_d^\lambda$ matrices (i.e., as computed without recourse to sinc DVR grid points)—thereby eliminating all quadrature error, and reducing the basis size still further, down to exactly the number used in classical calculations. In this context, the greatest challenge is posed by the fact that the exact matrices are no longer diagonal. Also, though still quite small by virtue of being two-dimensional, they are not quite small enough to satisfy our design conditions.

Despite the above challenges, we have developed an exact sinc QCC implementation that not only overcomes the non-diagonal limitation, but also satisfies both design conditions. This approach is based on the fact that the off-diagonal part of an exact $\hat{\gamma}$ matrix can be written in the form $\hat{\gamma}_{\text{offdiag}} = (\hat{p}_i\hat{p}_j\hat{D} + \hat{D}\hat{p}_i\hat{p}_j)/2$ —where \hat{D} is diagonal, and d subscripts (and λ superscripts) have been dropped for clarity. In the $\varepsilon \rightarrow 0$ limit, Trotterization then yields

$$\exp(-i\varepsilon\hat{\gamma}_{\text{offdiag}}) \approx \exp(-i\varepsilon\hat{p}_i\hat{p}_j\hat{D}/2)\exp(-i\varepsilon\hat{D}\hat{p}_i\hat{p}_j/2). \quad (18)$$

Note that the individual factors in Eq. (18) above are *no longer unitary*; the exponents are comprised of non-commutative *operator*—rather than tensor—products. Although some algorithms have come on the scene very recently,^{105,106} we have developed our own QCC implementation that is unitary, and correct to first order in ε . It involves separate *FT* operations for \hat{p}_1 and \hat{p}_2 , and also a two-dimensional function evaluation for \hat{D} —thereby satisfying our two design conditions. As this work is currently under review by Texas Tech University for possible patent protection, further details will be presented in a future publication.

Regardless of the particular CCS QCC implementation as described above, in all such cases the computational bottleneck is likely to be evaluation of the Gaussian or exponential function—which, like the inverse square-root described in Sec. 4.2, is currently regarded to be very expensive on quantum computers.^{56,95,104} Indeed, this cost could be so great as to render the various potential advantages of the CCS approach (e.g. the reduction in circuit complexity that might otherwise occur) largely moot, in practice.

To address this issue, we have concurrently developed a new algorithm for evaluating Gaussian and exponential functions efficiently on quantum computers—for which an additional TTU provisional patent has been filed. The algorithm is described and analyzed in great detail in a companion paper¹⁰⁴—not only in terms of gate and space complexity scalings, but also down to the level of specific Toffoli gate and qubit requirements. For most practical applications, the cost is the same as that of performing a handful of multiplications (with or without error correction), and is thus on a par with the other costs associated with the present CCS QCC algorithm.

Using the model CCS QCC parameters as described at the end of Sec. 4.1, the Toffoli count for Gaussian function evaluation is only 704, whereas that for the corresponding inverse square-root evaluation would be 134,302. Note that *in practice, the latter*

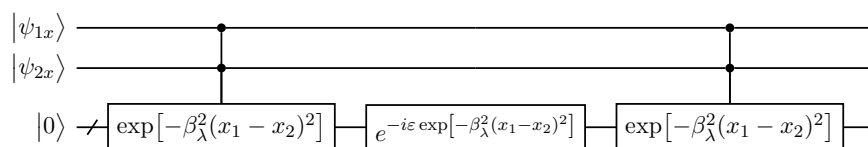


Fig. 5 CCS quantum circuit to implement $\exp(-i\epsilon\hat{\gamma}_x^\lambda)|\psi_{12x}\rangle$ on a quantum computer, in the sinc DVR. The function evaluation, $\gamma_x^\lambda = \exp[-\beta_\lambda^2(x_1 - x_2)^2]$, involves two explicit coordinates and sets of qubits, and includes an exponential function evaluation.

calculation would actually require more than the $n = 7$ qubits presumed here, as discussed in Sec. 4.2, so that the actual required Toffoli count would be even far greater than this (the scaling is $O(n^2)$ —which, with the more realistic $n = 10$ value, suggests an additional cost doubling).

5 Conclusions

The frontier in quantum chemistry calculations has always involved pushing the following limits: (a) full CI; (b) complete basis set (CBS); (c) number of explicit electrons, N . All of these imply a substantial increase in N_B , the basis size or number of Slater Determinants (SDs) needed to perform the calculation. Over the decades—but especially in the last 10 years or so—impressive and steady progress has been made towards increasing the number of SDs that can be treated explicitly in calculations.^{4,74–78,107–109} Much of the recent progress has relied on massive parallelization, but use of tensor decompositions of various kinds is also playing an increasingly important role. Moreover, going forward, it is clear that quantum computing—for which exponential growth in N_B corresponds to mere *linear* growth in the number of logical qubits—will engender an even greater sea change.^{5–35}

Whatever the future may bring, it seems that the quantum chemistry discipline may be at a “tipping point,” where there is once again room to consider bold new ideas. One such idea—that the electronic structure Hamiltonian operator separates more naturally by *Cartesian component* than by particle—represents a radical departure from the traditional particle-separated starting point, and serves as the focus of this work. In addition to directly addressing the traditional three limits, (a)–(c) above, the CCS approach also has ramifications for two additional quantum chemistry frontiers: (d) calculation of many excited states (including wavefunctions); (e) application to combined electron-nuclear motion quantum many-body problem. These latter two require $N_B \times N_B$ matrix *diagonalization* (as opposed to just calculation of the ground state), as well as the ability to go beyond traditional SD representations. Frontier (e) is, in addition, of special relevance for QCC.

In this study, we have sought to demonstrate the potential advantages presented by the CCS approach in both classical and quantum computing contexts. On the classical side, the CCS tensor-SOP decomposition of the wavefunction [Eq. (4)] enables astronomical basis sizes to be considered with minimal RAM requirements—e.g., $N_B \approx 10^{15}$ for the harmonium calculation performed in the present work, and up to $N_B \approx 10^{18}$ more generally. Of even greater import is the CCS tensor-SOP decomposition of the Hamiltonian operator itself, which reduces the complexity of both the classical and quantum calculations—essentially by re-

stricting the set of coordinates that must be considered at one time, from six down to two.

That said, on the quantum side, the overall computational bottleneck is presented by the evaluation of the appropriate function—i.e., the inverse square-root in the canonical first-quantized QCC case, or the Gaussian/exponential in the CCS QCC case. Using the new exponentiation algorithm as described in our companion paper,¹⁰⁴ the Toffoli count of the latter is found to be a factor of *200 times smaller* than the former, for a realistic model QCC example (Sec. 4.1). Moreover, that estimate assumes an equal number of qubits for both canonical and CCS calculations, when in reality, the former number is likely to be around 50% higher than the latter. Running in conjunction with the new exponentiation algorithm, then, the present CCS approach would appear to become a highly competitive contender for performing first-quantized QCC calculations, going forward.

In Sec. 4.3, we have presented two different CCS QCC Trotter implementations—i.e., the *exact non-diagonal sinc* option, and the *approximate diagonal sinc-DVR* option. Both of these represent an improvement over the standard canonical Trotter QCC implementation, in terms of both gate and space complexities, as discussed. In comparing the two CCS QCC implementations to each other, however, we find that the exact non-diagonal implementation requires more quantum gates, but fewer qubits, than the diagonal sinc-DVR alternative—thereby presenting a useful “engineering tradeoff.” A similar tradeoff is also available for the exponentiation algorithm itself.¹⁰⁴

We conclude by once again stressing the key point that *the full benefits of the CCS approach have yet to be realized*. This is because to date, all calculations have been performed using plane-wave and/or sinc basis functions, which represent a terrible choice for unscreened Coulomb systems. As discussed, something like $L \approx 100$ is required for such systems, corresponding to $M = L^3 = 10^6$ single-particle orbitals. For harmonium, plane waves are a reasonably good—but still not great—choice of basis. Here, we find a reduction to $L = 17$ or $M \approx 5000$. For the uniform or correlated electron gas application, plane waves are of course a much better choice, giving rise to $L = 11$, or $M \approx 1000$ orbitals. All of these are requirements for achieving chemical accuracy.

The main lesson here is the unsurprising one that *a suitable choice of CCS basis for a given application can lead to a dramatic reduction in basis size*. Ultimately, this should result in explicit classical calculations up to perhaps $N = 6$. Larger calculations could also be performed, using the output of a CCS calculation as a highly-efficient, multi-particle basis set (i.e., the N -particle, CCS version of a geminal basis set). Of course in practice, this will first require the development of the “optimal CCS basis” (OCCSB)

functions of the Eq. (1) form—i.e., the CCS analog of HF molecular orbitals.

As a technical matter, we advocate use of optimal separable basis theory^{84–86} to compute the OCCSB functions (rather than traditional SCF), because the result is an optimized, complete orthonormal basis obtained “all at once” (as opposed to a collection of non-orthogonal ground and excited state SCF functions obtained one at a time). In any event, and as mentioned several times, the individual OCCSB functions will incorporate correlation implicitly—thus potentially dramatically reducing the required basis size, even in cases where electron correlation is severe. At the same time, the CCS tensor decomposition enables classical computers to handle $N_B = 10^{15}$ or more basis functions, which is very promising.

Of course, OCCSB calculations have yet to be performed on classical computers, the era of first-quantized QCC is still a ways off, and it is never certain what the future will bring. Nevertheless, one thing already seems quite clear: it is best to have a variety of different methods in one’s computational arsenal—as indeed, has been the case within the confines of traditional second-quantized classical quantum chemistry for decades.

Conflicts of interest

There are no conflicts to declare.

Acknowledgements

This work was supported under contract from the US Army Research Office, Chemical Sciences Division (W911NF1910023). The Robert A. Welch Foundation (D-1523) also provided support. We also gratefully acknowledge a series of stimulating conversations with Ryan Babbush of Google Research. This technology is currently patent pending by the Texas Tech University System.

Appendix: First- and Second-Quantized Calculations, and the CCS Approach

In order to better understand the “first-” vs. “second-quantized” terminology in the context of QCC, it is helpful to consider the corresponding quantum *operators*, as distinct from their basis set representations. In the traditional first-quantized formalism, the Hamiltonian operator is expressed using electron position coordinates as indicated in Eq. (5).^{1–3} Of course for numerical purposes, this operator may be represented as a matrix using *any* desired representational basis set—i.e., any set of orthonormal functions on the entire $3N$ -dimensional “configuration space.” (Note that the latter phrase is being used in the generic sense to mean the space of all particle positions, rather than in the electronic structure sense of orbital occupations).

In particular, the basis functions need *not* be SDs. One obvious choice of basis that is decidedly not of the SD form is suggested by Eq. (5) itself—i.e., the position eigenstates. In principle, these are Dirac delta functions; in practice, due to basis set truncation, these are *sinc functions*,^{44–50} associated with a uniform lattice of grid points, and spanning the same Hilbert subspace as a corresponding band-limited set of plane waves. Both sinc (aka “plane-wave dual”) and plane-wave basis sets have been consid-

ered in the QCC context,^{13,24,26,35} and have also been employed with the CCS approach. However, many other CCS basis set are also possible—including those with substantial particle correlation “built in” to the individual basis functions (Sec. 2.3).

What is not built in to any first-quantized approach, however, is antisymmetry—which, as noted, must therefore be explicitly imposed. Here, the second-quantized approach has the upper hand, essentially because it treats operators and basis functions on an equal footing.³ In particular, second-quantized Hamiltonian operators are sums of products of creation and annihilation operators, acting on a set of $M \geq N$ single-particle (spin-)orbitals. Second quantized basis functions are “occupation number” (ON) vectors—i.e., binary strings denoting which of the M orbitals are occupied—spanning the 2^M -dimensional Fock space (in the “grand canonical” sense where N may vary, although for all of our applications, N is fixed). All ON vectors may be obtained by applying orbital-specific creation operators to the “vacuum state” of no electrons. The second-quantized approach is thus more abstract and algebraic than the first-quantized approach, although at the end of the day, *ON vectors always correspond to properly antisymmetrized SDs of single-particle orbitals*. This is both an advantage (because antisymmetrization need not be dealt with explicitly) and a disadvantage (because *no other* type of basis may be considered).

The CCS approach as advocated here does not rely on SDs, single-particle orbitals, nor particle separability of any kind. It is therefore very much a first-quantized approach, by any reckoning. Using the representational basis, the Hamiltonian operator is (implicitly) represented as an $N_B \times N_B$ matrix, which is then diagonalized. In principle, a large number of accurately converged eigenstates may be obtained, with rigorous variational convergence to the exact results guaranteed in the complete basis set (CBS) limit. The approach may therefore be compared with full-CI matrix diagonalization calculations from the second-quantized realm [i.e., for which all $N_B = \binom{M}{N}$ possible SDs are retained]. However, CCS calculations are *much* more flexible than full CI—not only with respect to the choice of basis itself, but also in terms of how the basis is truncated. More specifically, in a full-CI calculation, M is the only convergence parameter (with $M \rightarrow \infty$ defining the CBS limit). In contrast, in the CCS case, there are up to $3N$ (though usually just 3) separate basis truncation parameters, each of which can be adjusted independently for maximum efficiency.

There is one more advantage of the CCS approach that is particularly relevant, especially for QCC. Since it is not limited to SDs, it can be applied directly to the combined electron-nuclear motion quantum many-body problem. Ordinarily, one imposes the Born-Oppenheimer (BO) approximation,^{1,2} to separate the electronic and nuclear motion problems, although this introduces a source of error. More accurate results may therefore be obtained by solving the combined problem directly. In the QCC context however, there is a much more compelling and practical reason for wanting to solve the combined problem. This is because the BO approximation necessitates the development of an explicit potential energy surface (PES) over the entire $3N$ -dimensional space—a prospect which even on a quantum computer, scales exponen-

tially with N .^{14,17,35} By solving the combined electron-nuclear motion problem “all at once,” such PES problems are completely avoided—as are all BO-type errors.

The above considerations justify claims (a) thru (d) in Sec. 1, although additional arguments have also been provided throughout this paper.

Notes and references

- 1 A. Szabo and N. S. Ostlund, *Modern Quantum Chemistry: Introduction to advanced electronic structure theory*, Courier Corporation, 2012.
- 2 F. Jensen, *Introduction to Computational Chemistry*, John Wiley and Sons, Chichester, UK, 1999.
- 3 T. Helgaker, P. Jørgensen and J. Olsen, *Molecular Electronic-Structure Theory*, John Wiley and Sons, Chichester, UK, 2012.
- 4 J. Kong, C. A. White, A. I. Krylov, D. Sherrill, R. D. Adamson, T. R. Furlani, M. S. Lee, A. M. Lee, S. R. Gwaltney and T. R. Adams, *Journal of Computational Chemistry*, 2000, **21**, 1532–1548.
- 5 R. P. Poplavskii, *Usp. Fiz. Nauk.*, 1975, **115**, 465–501.
- 6 R. P. Feynman, *Int. J. Theor. Phys.*, 1982, **21**, 467–488.
- 7 S. Lloyd, *Science*, 1996, **273**, 1073–1078.
- 8 D. S. Abrams and S. Lloyd, *Phys. Rev. Lett.*, 1997, **79**, 2586–2589.
- 9 C. Zalka, *Proc. Royal Soc. London A*, 1998, **454**, 313.
- 10 D. A. Lidar and H. A. Wang, *Phys. Rev. E*, 1999, **59**, 2429.
- 11 D. S. Abrams and S. Lloyd, *Phys. Rev. Lett.*, 1999, **83**, 5162.
- 12 M. A. Nielsen and I. L. Chuang, *Quantum Computation and Quantum Information*, Cambridge Univ Press, 2000.
- 13 A. Aspuru-Guzik, A. D. Dutoi, P. J. Love and M. Head-Gordon, *Science*, 2005, **309**, 1704.
- 14 I. Kassal, S. P. Jordan, P. J. Love, M. Mohseni and A. Aspuru-Guzik, *Proc. Nat'l Acad. Sci.*, 2008, **105**, 18681.
- 15 J. D. Whitfield, J. Biamonte and A. Aspuru-Guzik, *arXiv preprint arXiv:1001.3885 [quant-ph]*, 2010.
- 16 K. L. Brown, W. J. Munro and V. M. Kendon, *Entropy*, 2010, **12**, 2268–2307.
- 17 O. Christiansen, *Phys. Chem. Chem. Phys.*, 2012, **14**, 6672.
- 18 I. M. Georgescu, S. Ashhab and F. Nori, *Rev. Mod. Phys.*, 2014, **86**, 153.
- 19 S. Kais, S. A. Rice and A. R. Dinner, *Quantum information and computation for chemistry*, John Wiley & Sons, 2014.
- 20 J. Huh, G. G. Guerreschi, B. Peropadre, J. R. McClean and A. Aspuru-Guzik, *Nature Photonics*, 2015, **9**, 615.
- 21 R. Babbush, *PhD thesis*, Harvard University, 2015.
- 22 I. D. Kivlichan, N. Wiebe, R. Babbush and A. Aspuru-Guzik, *J. Phys. A: Math Theo*, 2017, **50**, 305301.
- 23 R. Babbush, D. W. Berry, Y. R. Sanders, I. D. Kivlichan, A. Scherer, A. Y. Wei, P. J. Love and A. Aspuru-Guzik, *Quantum Sci. Technol.*, 2018, **3**, 015006.
- 24 R. Babbush, N. Wiebe, J. McClean, J. McClain, H. Neven and G. K.-L. Chan, *Phys. Rev. X*, 2018, **8**, 011044.
- 25 R. Babbush, C. Gidney, D. W. Berry, N. Wiebe, J. McClean, A. Paler, A. Fowler and H. Neven, *Phys. Rev. X*, 2018, **8**, 041015.
- 26 R. Babbush, D. W. Berry, J. R. McClean and H. Neven, *npj Quantum Information*, 2019, **5**, 92.
- 27 G. H. Low, N. P. Bauman, C. E. Granade, B. Peng, N. Wiebe, E. J. Bylaska, D. Wecker, S. Krishnamoorthy, M. Roetteler, K. Kowalski, M. Troyer and N. A. Baker, *arXiv preprint arXiv:1904.01131v1 [quant-ph]*, 2019.
- 28 I. D. Kivlichan, C. Gidney, D. W. Berry, N. Wiebe, J. McClean, W. Sun, Z. Jiang, N. Rubin, A. Fowler, A. Aspuru-Guzik, R. Babbush and H. Neven, *arXiv preprint arXiv:1902.10673*, 2019.
- 29 A. Izmaylov, T.-C. Yen and Ilya G. Ryabinkin, *Chemical Science*, 2019, **10**, 3746.
- 30 R. M. Parrish, E. G. Hohenstein, P. L. McMahan and T. J. Martinez, *arXiv preprint arXiv:1901.01234v1 [quant-ph]*, 2019.
- 31 E. Altman, K. R. Brown, G. Carleo, L. D. Carr, E. Demler, C. Chin, B. DeMarco, S. E. Economou, M. Eriksson and K.-M. Fu, *arXiv preprint arXiv:1912.06938*, 2019.
- 32 Y. Cao, J. Romero, J. P. Olson, M. Degroote, P. D. Johnson, M. Kieferova, I. D. Kivlichan, T. Menke, B. Peropadre, N. P. D. Sawaya, S. Sim, L. Veis and A. Aspuru-Guzik, *Chem. Reviews*, 2019, **119**, 10856.
- 33 Y. Alexeev, D. Bacon, K. R. Brown, R. Calderbank, L. D. Carr, F. T. Chong, B. DeMarco, D. Englund, E. Farhi and B. Fefferman, et al., *arXiv preprint arXiv:1912.07577*, 2019.
- 34 B. Bauer, S. Bravyi, M. Motta and G. K. Chan, *arXiv preprint arXiv:2001.03685*, 2020.
- 35 S. McArdle, S. Endo, A. Aspuru-Guzik, S. Benjamin and X. Yuan, *Rev. Mod. Phys.*, 2020, 15003.
- 36 T. Dresselhaus, C. B. A. Bungey, P. J. Knowles and F. R. Manby, *J. Chem. Phys.*, 2020, **153**, 214114.
- 37 J. Preskill, *arXiv preprint arXiv:1801.00862v3 [quant-ph]*, 2018.
- 38 K. Bharti, A. Cervera-Lierta, T. H. Kyaw, T. Huag, S. Alperin-Lea, A. Anand, M. Degroote, H. Heimonen, J. S. Kottmann, T. Menke, W.-K. Mok, S. Sim, L.-C. Kwek and A. Aspuru-Guzik, *arXiv preprint arXiv:2101.08448v1 [quant-ph]*, 2021.
- 39 P.-O. Löwdin and H. Shul, *Phys. Rev.*, 1956, **101**, 1730.
- 40 D. M. Silver, *J. Chem. Phys.*, 1969, **50**, 5108.
- 41 A. Gonis and T. C. Schulthess, *J. Phys.: Condensed Matter*, 1998, **10**, 3535.
- 42 D. A. Mazziotti, *J. Chem. Phys.*, 2000, **112**, 10125.
- 43 D. A. Mazziotti, *Phys. Rev. A*, 2010, **81**, 062515.
- 44 F. Stenger, *Numerical methods based on sinc and analytic functions*, Springer, New York, 1993.
- 45 D. T. Colbert and W. H. Miller, *J. Chem. Phys.*, 1992, **96**, 1982–1990.
- 46 V. Szalay, *J. Chem. Phys.*, 1996, **105**, 6940.
- 47 J. C. Light and T. Carrington Jr., *Adv. Chem. Phys.*, 2000, **114**, 263.
- 48 R. G. Littlejohn, M. Cargo, T. Carrington, Jr., K. A. Mitchell and B. Poirier, *J. Chem. Phys.*, 2002, **116**, 8691–8703.

- 49 R. G. Littlejohn and M. Cargo, *J. Chem. Phys.*, 2002, **116**, 7350.
- 50 J. Jerke, Y. Lee and C. J. Tymczak, *J. Chem. Phys.*, 2015, **143**, 064108.
- 51 J. O’Gorman and E. T. Campbell, *Phys. Rev. A*, 2017, **95**, 032338.
- 52 D. W. Berry, A. M. Childs, R. Cleve, R. Kothari and R. D. Somma, Proceedings of the Forty-sixth Annual ACM Symposium on Theory of Computing, New York, NY, 2014, pp. 283–292.
- 53 G. H. Low and I. L. Chuang, *arXiv preprint arXiv:1610.06546*, 2016.
- 54 D. W. Berry, C. Gidney, M. Motta, J. R. McClean and R. Babbush, *Quantum*, 2019, **3**, 208.
- 55 D. W. Berry, A. M. Childs, Y. Su, X. Wang and N. Wiebe, *arXiv preprint arXiv:1906.07115*, 2019.
- 56 R. Babbush, (private communication).
- 57 J. Jerke and B. Poirier, *J. Chem. Phys.*, 2018, **148**, 104101.
- 58 J. Jerke, J. Karwowski and B. Poirier, *Mol. Phys.*, 2019, **117**, 1264–1275.
- 59 C. Coulson and A. Neilson, *Proc. Phys. Soc.*, 1961, **78**, 831.
- 60 D. M. Ceperley and B. J. Alder, *Phys. Rev. Lett.*, 1980, **45**, 566.
- 61 R. Esteban, A. G. Borisov, P. Nordlander and J. Aizpurua, *Nature Comm.*, 2012, **3**, 825.
- 62 A. Varas, P. García-González, J. Feist, F. García-Vidal and A. Rubio, *Nanophotonics*, 2016, **5**, 409–426.
- 63 J. Jerke, E. R. Bittner and B. Poirier, (in preparation).
- 64 J. F. Pérez-Torres, *Phys. Rev. A*, 2013, **87**, 062512.
- 65 J. Liu, E. J. Salumbides, U. Hollenstein, J. C. J. Koelemeij, K. S. E. Eikema, W. Ubachs and F. Merkt, *J. Chem. Phys.*, 2009, **130**, 174306.
- 66 J. Karwowski and K. Szewc, *Collection of Czechoslovak Chemical Communications*, 2008, **73**, 1372.
- 67 J. Karwowski and L. Cyrnek, *Annalen der Physik*, 2004, **13**, 181.
- 68 J. Karwowski and H. A. Witek, *Theo. Chem. Acc.*, 2014, **133**, 1494.
- 69 H. F. Trotter, *Proc. Am. Math. Soc.*, 1959, **10**, 545.
- 70 P. W. Shor, Proc. 35th Ann. Symp. on Found. Comp. Sci., Los Alamitos, CA, 1994.
- 71 G. Beylkin and M. J. Mohlenkamp, *SIAM Journal on Scientific Computing*, 2005, **26**, 2133–2159.
- 72 V. Khoromskaia and B. N. Khoromskij, *Physical Chemistry Chemical Physics*, 2015, **17**, 31491–31509.
- 73 A. Leclerc and T. Carrington, Jr., *Chem. Phys. Lett.*, 2016, **644**, 183.
- 74 E. G. Hohenstein, R. M. Parrish and T. J. Martínez, *J. Chem. Phys.*, 2012, **137**, 044103.
- 75 R. M. Parrish, E. G. Hohenstein, N. F. Schunck, C. D. Sherrill and T. J. Martínez, *Phys. Rev. Lett.*, 2013, **111**, 132505.
- 76 R. Shepard, G. Gidofalvi and S. R. Brozell, *J. Chem. Phys.*, 2014, **141**, 064105.
- 77 R. Shepard and S. R. Brozell, *Mol. Phys.*, 2019, **117**, 2374.
- 78 H. L. et. al, *J. Chem. Phys.*, 2020, **152**, 134110.
- 79 J. Rys, M. Dupuis and H. F. King, *J. Comp. Chem.*, 1983, **4**, 154.
- 80 D. J. Klein, C. H. Carlisle and F. A. Matsen, *Adv. Quant. Chem.*, 1970, **5**, 219.
- 81 E. Rytter, *Chem. Phys.*, 1976, **12**, 355.
- 82 D. R. Herrick, *Adv. Chem. Phys.*, 1983, **52**, 1.
- 83 W. M. McClain, *Symmetry Theory in Molecular Physics with Mathematica*, Springer, New York, 2008.
- 84 B. Poirier, *Phys. Rev. A*, 1997, **56**, 120–130.
- 85 B. Poirier and J. C. Light, *J. Chem. Phys.*, 1999, **111**, 4869–4885.
- 86 B. Poirier, *Numer. Linear Algebra Appl.*, 2000, **7**, 715–726.
- 87 X.-G. Wang and T. Carrington, Jr., *J. Chem. Phys.*, 2001, **114**, 1473.
- 88 J. Montgomery and B. Poirier, *J. Chem. Phys.*, 2003, **119**, 6609.
- 89 D. W. Berry, M. Kieferova, A. Scherer, Y. R. Sanders, G. H. Low, N. Wiebe, C. Gidney and R. Babbush, *npj Quantum Information*, 2018, **4**, 22.
- 90 C. Lanczos, *An iteration method for the solution of the eigenvalue problem of linear differential and integral operators*, United States Government Press Office, Los Angeles, CA, 1950.
- 91 T. G. Draper, *arXiv preprint arXiv:2000.0008033 [quant-ph]*, 2000.
- 92 G. Florio and D. Picca, *arXiv preprint arXiv:2004.0403048v1 [quant-ph]*, 2004.
- 93 G. Florio and D. Picca, *arXiv preprint arXiv:2004.0407079 [quant-ph]*, 2004.
- 94 T. Häner, M. Roetteler and K. M. Svore, *Quantum Information and Computation*, 2017, **18**, 673–684.
- 95 T. Häner, M. Roetteler and K. M. Svore, *arXiv preprint arXiv:1805.12445v1 [quant-ph]*, 2018.
- 96 Y. R. Sanders, D. W. Berry, P. C. Costa, L. W. Tessler, N. Wiebe, C. Gidney, H. Neven and R. Babbush, *Phys. Rev. X Quantum*, 2020, **1**, 020312.
- 97 A. Parent, M. Roetteler and M. Mosca, 12th Conference on the Theory of Quantum Computation, Communication, and Cryptography (TQC 2017), Germany, 2017, pp. 7:1–7:15.
- 98 C. Gidney, *arXiv preprint arXiv:1904.07356v1 [quant-ph]*, 2019.
- 99 A. Karatsuba and Y. Ofman, *Doklady Akad. Nauk SSSR*, 1962, **145**, 293–294.
- 100 L. A. B. Kowada, R. Portugal and C. M. H. de Figueiredo, *Journal of Universal Computer Science*, 2006, **12**, 499–511.
- 101 S. A. Cuccaro, T. G. Draper, S. A. Kutin and D. P. Moulton, *arXiv preprint arXiv:quant-ph/0410184*, 2004.
- 102 Y. Takahashi, *PhD thesis*, The University of Electro-Communications, 2008.
- 103 Y. Takahashi, S. Tani and N. Kunihiro, *arXiv preprint arXiv:0910.2530v1 [quant-ph]*, 2009.
- 104 B. Poirier, *Phys. Rev. X Quantum*, (submitted).

- 105 S. E. Rasmussen and N. T. Zinner, *arXiv preprint arXiv:2002.11728v2 [quant-ph]*, 2020.
- 106 S. Endo, J. Sun, Y. Li, S. C. Benjamin and X. Yuan, *Phys. Rev. Lett.*, 2020, **125**, 010501.
- 107 T. Müller, *J. Phys. Chem. A*, 2009, **113**, 12729.
- 108 W. A. de Jong *et al*, *Phys. Chem. Chem. Phys.*, 2010, **12**, 6896.
- 109 K. D. Vogiatzis, D. Ma, J. Olsen, L. Gagliardi and W. A. de Jong, *J. Chem. Phys.*, 2017, **147**, 184111.